Theoretical Study of the Gas-Phase Reactions of Iodine Atoms ($^2P_{3/2}$) with H_2, H_2O, HI, and OH

Sébastien Canneaux,[†,§] Bertrand Xerri,[‡,§] Florent Louis,*[,†,§] and Laurent Cantrel[‡,§]

PhysicoChimie des Processus de Combustion et de l'Atmosphère (PC2A), UMR 8522 CNRS/Lille1, Université Lille 1 Sciences et Technologies, Cité scientifique, Bât C11/C5, 59655 Villeneuve d'Ascq Cedex, France, Institut de Radioprotection et de Sûreté Nucléaire, DPAM, Centre de Cadarache, BP3, 13115 Saint Paul Lez Durance Cedex, France, and Laboratoire de Recherche Commun IRSN-CNRS-Lille1 "Cinétique Chimique, Combustion, Réactivité" (C^3R), Centre de Cadarache, BP3, 13115 Saint Paul Lez Durance Cedex, France

Received: May 7, 2010; Revised Manuscript Received: July 5, 2010

The rate constants of the reactions of iodine atoms with H_2, H_2O, HI, and OH have been estimated using 39, 21, 13, and 39 different levels of theory, respectively, and have been compared to the available literature values over the temperature range of 250−2500 K. The aim of this methodological work is to demonstrate that standard theoretical methods are adequate to obtain quantitative rate constants for the reactions involving iodine-containing species. Geometry optimizations and vibrational frequency calculations are performed using three methods (MP2, MPW1K, and BHandHLYP) combined with three basis sets (cc-pVTZ, cc-pVQZ, and 6-311G(d,p)). Single-point energy calculations are performed with the highly correlated ab initio coupled cluster method in the space of single, double, and triple (pertubatively) electron excitations CCSD(T) using the cc-pVnZ (n = T, Q, and 5), aug-cc-pVnZ (n = T, Q, and 5), 6-311G(d,p), 6-311+G(3df,2p), and 6-311++G(3df,3pd) basis sets. Canonical transition state theory with a simple Wigner tunneling correction is used to predict the rate constants as a function of temperature. CCSD(T)/cc-pVnZ//MP2/cc-pVTZ (n = T and Q), CCSD(T)/6-311+G(3df,2p)//MP2/6-311G(d,p), and CCSD(T)/6-311++G(3df,3pd)//MP2/6-311G(d,p) levels of theory provide accurate kinetic rate constants when compared to available literature data. The use of the CCSD(T)/cc-pVQZ//MP2/cc-pVTZ and CCSD(T)/6-311++G(3df,3pd) levels of theory allows one to obtain a better agreement with the literature data for all reactions with the exception of the I + H_2 reaction R_1. This computational procedure has been also used to predict rate constants for some reactions where no available experimental data exist. The use of quantum chemistry tools could be therefore extended to other elements and next applied to develop kinetic networks involving various fission products, steam, and hydrogen in the absence of literature data. The final objective is to implement the kinetics of gaseous reactions in the ASTEC (Accident Source Term Evaluation Code) code to improve speciation of fission transport, which can be transported along the Reactor Coolant System (RCS) of a Pressurized Water Reactor (PWR) in case of a severe accident.

I. Introduction

During a loss-of-coolant accident due to a break in the Reactor Coolant System (RCS) of a nuclear Pressurized Water Reactor (PWR), part of the nuclear fuel could melt, and released fission products would be transported through the RCS and its break to the reactor containment building and then possibly to the environment. Radioiodine is one of the most radiotoxic fission products that could be released from the fuel due to its ability to form volatile species,[1] and the potential accidental release of volatile iodine to the environment is a key safety issue for emergency response planning.[2] Many experimental and theoretical programs[3−6] have been devoted to characterize the behavior of iodine from the fuel to the environment. One of the main uncertainties is related to the speciation of iodine in the RCS. Due to its high reactivity, iodine has indeed been observed to be transported in the RCS in various forms, including aerosol, vapors, or gas, and to be combined with other fission products. The gaseous part of iodine at the break has a great impact on the potential iodine outside releases, and kinetic limitations are suspected to promote iodine gaseous species. To predict the gaseous iodine quantity reaching the containment building, depending on accident scenarios, the thermokinetic parameters of the main gaseous reactions which govern the overall iodine behavior in the RCS have to be determined. A theoretical approach using quantum chemistry tools has been carried out to estimate accurately the thermokinetic parameters for the main reactions involving iodine-containing species as described in this paper. Quantum chemistry appears also to be a supporting and promising tool to interpret the future experimental results coming from the International Source Term Program[6] (ISTP), conducted by the French Institute for Radiological and Nuclear Safety (Institut de Radioprotection et de Sûreté Nucléaire, IRSN).

This work contributes to a detailed kinetic model-making which will incorporate iodine-containing species and could be later implemented in the ASTEC[7]/SOPHAEROS[8] severe accident simulation software. In a first step, this work has been restricted to some relevant reactions[9] occurring in the RCS

* To whom correspondence should be addressed. Phone: (33)3-20436977. E-mail: florent.louis@univ-lille1.fr.
† Université Lille 1 Sciences et Technologies.
‡ Institut de Radioprotection et de Sûreté Nucléaire.
§ Laboratoire de Recherche Commun IRSN-CNRS-Lille1 "Cinétique Chimique, Combustion, Réactivité" (C^3R).

10.1021/jp104163t
Published on Web 07/30/2010

$$I\,(^2P_{3/2}) + H_2 \rightarrow HI + H \qquad (R_1)$$

$$HI + H \rightarrow I\,(^2P_{3/2}) + H_2 \qquad (R_{-1})$$

$$I\,(^2P_{3/2}) + H_2O \rightarrow HI + OH \qquad (R_2)$$

$$HI + OH \rightarrow I\,(^2P_{3/2}) + H_2O \qquad (R_{-2})$$

$$I\,(^2P_{3/2}) + HI \rightarrow H + I_2 \qquad (R_3)$$

$$H + I_2 \rightarrow I\,(^2P_{3/2}) + HI \qquad (R_{-3})$$

$$I\,(^2P_{3/2}) + OH \rightarrow HI + O\,(^3P) \qquad (R_4)$$

$$HI + O\,(^3P) \rightarrow I\,(^2P_{3/2}) + OH \qquad (R_{-4})$$

The choice of these species (H_2, H_2O, HI, and OH) is mainly dictated by the presence of these species in the RCS in the case of a severe accident.

One of the most difficult problems from the experimental point of view is the direct determination of the temperature dependence of the kinetics of these reactions over a temperature range wide enough to include thermal oxidation and combustion processes. Most of the time, scientists rely on extrapolations based on relatively low temperature measurements (298−1500 K) combined with modeling in order to estimate rate constant values corresponding to combustion temperatures (1500−2500 K). However, the extrapolation procedure does not take into account possible changes in the mechanisms with the temperature and tunneling effects that might significantly decrease as the temperature increases. In addition, most of the experimental measurements just provide overall rate constants and do not give details of the temperature dependence of the mechanisms and kinetics of the individual pathways involved in the reaction. Quantum chemical calculations in conjunction with Transition State Theory (TST) can assess the relative importance of the elementary reactions as a function of temperature, like the ones described in the eight studied reactions, without the need for empirical and complicated extrapolation procedures based on low-temperature data.

In this work, quantum chemistry calculations and TST kinetic models are used to compute the temperature dependence of the rate constants for the abstraction reactions by iodine atoms. Experimental measurements, evaluation and estimation data, and theoretical studies have been previously reported in the literature.[10−29] Table 1 summarizes the available literature results together with the corresponding references. To our knowledge, there are no kinetic data available in the literature for the reactions R_2 and R_4. In the case of the reaction R_1 between iodine atoms and H_2, Inada and Akagane[11] reported calculations using the QCISD method with the Dunning−Huzinaga valence double-ζ basis set (D95V) supplemented by polarization functions to compute rate constants in the temperature range of 298−1500 K. The Arrhenius activation energy for reaction R_1 was also estimated by Truhlar and Gray[12] using

TABLE 1: Literature Rate Parameters for the Studied Reactions

reaction	A, cm^3 molecule^{-1} s^{-1}	E_a, kJ mol^{-1}	k, cm^3 molecule^{-1} s^{-1}	T, K	methods	references
$I\,(^2P_{3/2}) + H_2 \rightarrow HI + H$ (R_1)	$(3.92 \pm 1.15) \times 10^{-9}$	178.0 ± 5.47		1755−2605	ST[a]	Michael et al., 2000 (ref 10)
		143.1	2.4×10^{-35}	298	theory[b]	Inada and Akagane, 1996 (ref 11)
			2.0×10^{-17}	1000		
			1.1×10^{-14}	1500		
		138.9		300	theory[c]	Truhlar and Gray, 1978 (ref 12)
			7.64×10^{-18}	973	experiment[d]	Horie et al., 1964 (ref 13)
	$1.02 \times 10^{-10}\,(T/298\ \mathrm{K})^{0.50}$	137.0 ± 1.0		667−800	T/P[e]	Sullivan, 1962 (ref 14)
	$1.61 \times 10^{-10}\,(T/298\ \mathrm{K})^{0.50}$	140.0		633−738	T/P[e]	Sullivan, 1959 (ref 15)
	$(4.52 \pm 0.34) \times 10^{-10}$	142.0 ± 0.28		230−2605	evaluation	Michael et al., 2000 (ref 10)
	2.81×10^{-10}	141.0		600−1000	evaluation	Baulch et al., 1981 (ref 16)
$HI + H \rightarrow I\,(^2P_{3/2}) + H_2$ (R_{-1})			2.09×10^{-11}	298	EB/MS[f]	Vasileiadis and Benson, 1997 (ref 17)
	6.08×10^{-11}	3.00		230−297	U/vis−UV[g]	Umemoto et al., 1988 (ref 18)
	7.41×10^{-11}	2.41		250−373	EB/RF[h]	Lorenz et al., 1979 (ref 19)
	7.87×10^{-11}	2.74		600−1000	evaluation	Baulch et al., 1981 (ref 16)
$HI + OH \rightarrow I\,(^2P_{3/2}) + H_2O$ (R_{-2})			7.0×10^{-11} $(T/298\ \mathrm{K})^{-1.5}$	246−353	FP/RF[i]	Campuzano-Jost and Crowley, 1999 (ref 20)
			3.3×10^{-11}	298	EB/ESR[j]	Lancar et al., 1991 (ref 21)
			2.71×10^{-11}	298	FP/RF[i]	Mac Leod et al., 1990 (ref 22)
			9.0×10^{-12}	295	FP/vis−UV[k]	Smith and Zellner, 1974 (ref 23)
			1.3×10^{-11}	295	EB/ESR[j]	Takacs and Glass, 1973 (ref 24)
	1.6×10^{-11}	−3.66		240−360	evaluation	Atkinson et al., 2007 (ref 25)
			3.0×10^{-11}	298	evaluation	Sander et al., 2006 (ref 26)
			1.15×10^{-11}	298	evaluation	Baulch et al., 1981 (ref 16)
$I\,(^2P_{3/2}) + HI \rightarrow H + I_2$ (R_3)	1.33×10^{-9}	155.4		300−1000	theory[l]	Garrett and Truhlar, 1979 (ref 27)
	9.12×10^{-12}	(150.3 ± 2.1)		633−738	estimation	Sullivan, 1959 (ref 15)
			4.37×10^{-18}	1000	evaluation	Baulch et al., 1981 (ref 16)
$H + I_2 \rightarrow I\,(^2P_{3/2}) + HI$ (R_{-3})	$(6.59 \pm 1.99) \times 10^{-10}$	0.17		250−423	EB/RF[h]	Lorenz et al., 1979 (ref 19)
	7.16×10^{-10}	1.80		600−800	evaluation	Baulch et al., 1981 (ref 16)
$HI + O\,(^3P) \rightarrow I\,(^2P_{3/2}) + OH$ (R_{-4})	$(4.68 \pm 0.47) \times 10^{-11}$	8.31 ± 0.33		298−554	P/C[m]	Singleton and Cvetanovic, 1978 (ref 28)
	1.76×10^{-11}	5.93		200−500	theory[n]	Persky and Broida, 1987 (ref 29)

[a] ST: Shock Tube. [b] Based on ab initio calculations and transition state theory. [c] Based on the computation of Tolman Energy of activation using quantum mechanical transition probabilities. [d] Experiment where data are derived from detailed balance/reverse rate. [e] T/P: Thermal excitation technique/Pressure measurement as analytical technique. [f] EB/MS: Electron Beam/Mass Spectrometry. [g] U/vis−UV: Ultrasonics/vis−UV absorption. [h] EB/RF: Electron Beam/Resonance Fluorescence. [i] FP/RF: Flash Photolysis/Resonance Fluorescence. [j] EB/ESR: Electron Beam/Electron Spin Resonance. [k] FP/vis−UV: Flash Photolysis/vis−UV absorption. [l] Based on the Bond Energy−Bond Order (BEBO) method. [m] P/C: Photolysis/Chemiluminescence. [n] Based on a quasiclassical trajectory study.

quantum mechanical transition probabilities. In the case of the reaction R_3, a theoretical study[27] based on the BEBO method (Bond Energy−Bond Order) has been reported in the literature, leading to an estimation of the Arrhenius parameters over the temperature range of 300−1000 K. Persky and Broida[29] performed quasiclassical trajectory studies to determine the temperature dependence of the rate constants over the temperature range of 200−500 K.

In this study, highly correlated ab initio quantum chemistry and density functional theory calculations were performed in order to directly compute the reaction barriers for the considered reactions without any further adjustment of the energy. The energetics of these reactions was used together with TST calculations to compute rate constants in the temperature range of 250−2500 K. This is the first time, except for the reaction R_1, that the barriers for these reactions are computed directly using theoretical methods without recurring empirical fitting schemes or indirect methods involving isodesmic reactions.

This article is organized as follows. Computational methods are reported in section II, while the results are presented and discussed in section III.

II. Computational Methods

A wide variety of methods, described hereafter, have been used with the objective to select a more reliable method able to compute accurately the thermokinetic parameters for the iodine reactions, and next, maybe we could apply this methodology to other reactions involving fission products like cesium, for instance.

Ab initio and DFT calculations were performed using the GAUSSIAN03[30] software package. Reactants, transition states (TSs), molecular complexes, and products were fully optimized with the MP2,[31] MPW1K,[32] and BHandHLYP[33] methods using two Dunning's correlation-consistent basis sets[34] (cc-pVTZ and cc-pVQZ) and the Pople-type 6-311G(d,p) basis set.[35] For the iodine atom, we used the cc-pVnZ-PP (n = T and Q) basis sets of Peterson et al.,[36] which incorporate a relativistic pseudopotential (effective core potential) that largely accounts for scalar relativistic effects in iodine (these basis sets will be written without the PP term throughout the paper). We also employed an all-electron 6-311G basis[37] with valence basis sets augmented by the polarization d function.[38] All TSs have been characterized by one imaginary frequency (first-order saddle points) on the Potential Energy Surface (PES). Special care was taken to determine Minimum Energy Pathways (MEPs), performing Intrinsic Reaction Coordinate analyses (IRC)[39] at all levels of theory, in order to confirm that a specific TS connects the different local minima. Vibrational frequencies and Zero-Point vibrational Energies (ZPE) were determined within the harmonic approximation, at the same level of theory as that for geometries. The ab initio and DFT vibrational frequencies were multiplied by an appropriate scaling factor, which was obtained at each level of theory by plotting observed fundamentals for H_2, OH, HI, I_2, and H_2O versus calculated frequencies. Their values are given in the Table 1S of the Supporting Information. For all stationary points (reactants, TS, molecular complexes, and products), single-point energy calculations were carried out at different high levels of theory using, in each case, the optimized MP2, MPW1K, and BHandHLYP geometrical parameters. Electronic energies were obtained by employing the single and double coupled cluster theory with inclusion of a perturbative estimation for triple excitation (CCSD(T))[40] using (i) the cc-pVnZ and aug-cc-pVnZ (n = T, Q, and 5) basis sets on geometries previously optimized with the Dunning-type basis sets and (ii) the 6-311G(d,p), the 6-311+G(3df,2p), and 6-311++G(3df,3pd) basis sets[35,38] on geometries obtained with the Pople-type 6-311G(d,p) basis set. The frozen-core approximation has been applied in CCSD(T) calculations, which implies that the inner shells are excluded at estimating the correlation energy.

Spin−orbit coupling is of crucial importance, especially in the case of halogen atoms.[41,42] The potential energy of the iodine atom I ($^2P_{3/2}$) was obtained by subtracting one-third of the $^2P_{3/2} - {}^2P_{1/2}$ experimental splitting of the iodine atom[43] (30.29 kJ mol^{-1}) from the potential energy of the iodine atom I (^2P). Potential energies of the molecular complexes (MCR1, MCR2, MCR3, and MCR4) in the channel where the iodine atom ($^2P_{3/2}$) is separated from H_2, H_2O, HI, and OH were also modified by subtracting 30.29 kJ mol^{-1} from their potential energies. The spin−orbit corrections to the potential energies of HI, I_2, OH, and O (^3P) are −2.09,[44] −6.82,[45] −0.83,[46] and −0.93[43] kJ mol^{-1}, respectively, while the potential energies of molecular complexes (MCP1, MCP2, MCP3, and MCP4) incorporate the spin−orbit corrections corresponding to the reaction products. In the TSs, the spin−orbit interaction is made negligibly small by delocalization of spin from the I atom. Similar results have been obtained for TS structures in the reaction of O (^3P) with C_2H_5I.[47]

The rate coefficient k for the reactions under study involving a hydrogen-bonded adduct was initially analyzed according to the scheme advocated by Singleton and Cvetanovic[48] for prereactive complexes. We assume here that the reactions occur according to the mechanism involving a fast pre-equilibrium between the reactants and the prereactive complex (first step) followed by an abstraction leading to the postreactive complex and the products (second step). If k_1 and k_{-1} are the rate constants for the first step and k_2 corresponds to the second step, a steady-state analysis leads to a rate constant for the overall reaction, which can be written as

$$k = \frac{k_1 k_2}{k_{-1}} = \left(\frac{A_1 A_2}{A_{-1}}\right) \exp(-(E_1 + E_2 - E_{-1})/RT) \quad \text{(II-1)}$$

Since E_1 is 0, the net vibrationally adiabatic barrier E_0 for the overall reaction is given by the following relation

$$E_0 = E_2 - E_{-1} = (E_{TS} - E_{MCR}) - (E_R - E_{MCR}) + (ZPE_{TS} - ZPE_{MCR}) - (ZPE_R - ZPE_{MCR})$$
$$E_0 = E_{TS} - E_R + (ZPE_{TS} - ZPE_R) \quad \text{(II-2)}$$

where E_R, E_{MCR}, and E_{TS} are the potential energies of the reactants, the prereactive complex, and the TS, respectively, whereas ZPE_R, ZPE_{MCR}, and ZPE_{TS} are their corresponding Zero-Point Energy corrections. Thus, the vibrationally adiabatic barrier at high pressures can be calculated as the difference between the energy of the TS and the energy of the reactants, without having to obtain the prereactive complex. Applying basic statistical thermodynamic principles, the equilibrium constant K_{R-MCR} of the fast pre-equilibrium between the reactants and the prereactive complex may be obtained as

$$K_{R-MCR} = \frac{Q_{MCR}}{Q_R} \exp[((E_R + ZPE_R) - (E_{MCR} + ZPE_{MCR}))/RT] \quad \text{(II-3)}$$

where Q_R and Q_{MCR} are the total partition functions of the reactants and the prereactive complex, respectively. Under high-pressure conditions, an equilibrium distribution of reactants is maintained in a unimolecular process, and the classical TST formula can be applied[49] to calculate k_2

$$k_2(T) = \Gamma(T) \times \frac{k_B T}{h} \times \frac{Q_{TS}(T)}{Q_{MCR}(T)} \times \exp\left(\frac{(E_{MCR} + ZPE_{MCR}) - (E_{TS} + ZPE_{TS})}{k_B T}\right) \quad \text{(II-4)}$$

where $\Gamma(T)$ indicates the transmission coefficient used for the tunneling correction at temperature T, k_B is Boltzmann's constant, and h is Planck's constant.

The reaction path degeneracy is not included in this expression since the rotational symmetry numbers are already introduced in the calculation of the partition functions. The calculation of the reaction rate constants using the TST formulation given by eq II-4 requires the proper computation of the partition functions of the prereactive complex and the TS. The total partition function $Q^X(T)$ of a species X can be cast in terms of the translational $Q^X_{trans}(T)$, electronic $Q^X_{elec}(T)$, rotational $Q^X_{rot}(T)$, and vibrational $Q^X_{vib}(T)$ partition functions

$$Q^X(T) = Q^X_{trans}(T) Q^X_{elec}(T) Q^X_{rot}(T) Q^X_{vib}(T) \quad \text{(II-5)}$$

In this work, we adopt the simple and computationally inexpensive Wigner method[50] in the calculation of all tunneling corrections for the reactions reported here

$$\Gamma(T) = 1 + \frac{1}{24}\left(\frac{h|\nu^{\neq}|}{k_B T}\right)^2 \quad \text{(II-6)}$$

where $|\nu^{\neq}|$ is the module of the imaginary frequency at the saddle point. In the case of the reactions of iodine atoms with H_2, H_2O, and HI, this choice seems to be appropriate to the tunneling corrections applied to rate constants over the temperature range of 250−2500 K, for which the values of transmission coefficients $\Gamma(T)$ are small to moderate (≤ 2).[51] In the case of the reaction of iodine atoms with OH, the $\Gamma(T)$ values are more important but still less than a factor of 6 at 250 K. More sophisticated and computationally demanding algorithms such as the ones developed by Truhlar[52] and Miller[53] should be used if the transmission coefficients are much higher than the ones computed in this study. The rate constant calculations were performed over the temperature range of interest using the KISTHEP software suite.[54]

The rate constants of the reactions of iodine atoms with H_2O (reaction R_2), HI (reaction R_3), and OH (reaction R_4) are calculated as described above. In the case of the reaction of iodine atoms with H_2 (reaction R_1), although the prereactive complex structure has been located on the PES at all levels of theory, the relative enthalpies calculated at 0 K exhibit small differences by comparison to the reactants (<-2 kJ mol^{-1}). In the case of reaction R_1, canonical TST[49] is used to predict the temperature dependence of the rate constants. Accordingly, the rate constants $k(T)$ are computed using the following expression

$$k(T) = \Gamma(T) \times \frac{k_B T}{h} \times \frac{Q_{TS1}(T)}{Q_I(T) Q_{H_2}(T)} \times \exp\left(-\frac{E_0}{k_B T}\right) \quad \text{(II-7)}$$

where the terms $Q_{TS1}(T)$, $Q_I(T)$, and $Q_{H_2}(T)$ are the total partition functions for the TS1, the iodine atom, and the molecular hydrogen at the temperature T. In eq II-7, the vibrationally adiabatic barrier height, E_0, is computed as the energy difference between the TS1 and the reactants I and H_2.

The rate constants of the reverse reactions are obtained using the following expression

$$k_{reverse}(T) = k_{forward}(T) \times K_{eq}(T) \quad \text{(II-8)}$$

where $K_{eq}(T)$ is the equilibrium constant between the reactants and the products. $K_{eq}(T)$ is calculated at the same level of theory as $k_{forward}(T)$.

III. Results and Discussion

1. Geometric Parameters and Vibrational Frequencies. Figures 1−4 show the structures and atom numbering of the determined TSs and molecular complexes for the four studied

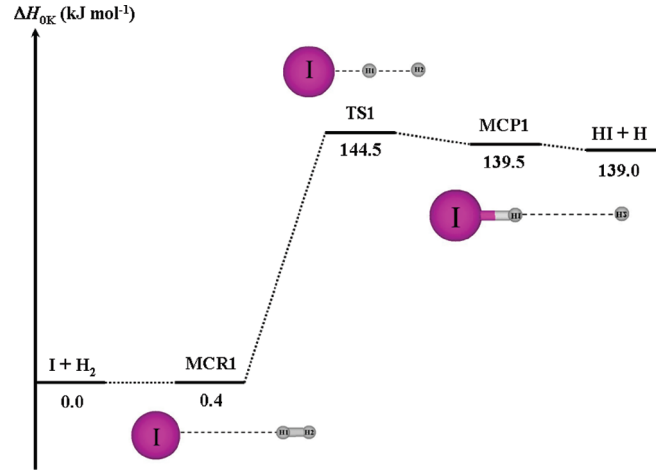

Figure 1. Potential energy profiles for the I ($^2P_{3/2}$) + H_2 reaction system calculated at the CCSD(T)/cc-pVTZ//MP2/cc-pVTZ level of theory.

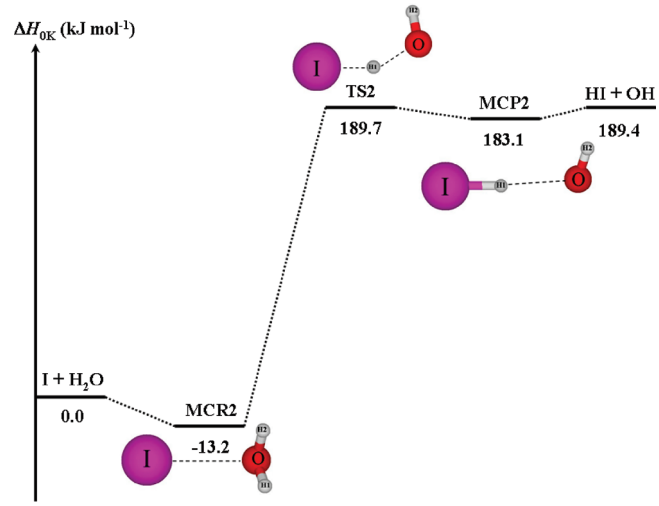

Figure 2. Potential energy profiles for the I ($^2P_{3/2}$) + H_2O reaction system calculated at the CCSD(T)/cc-pVTZ//MP2/cc-pVTZ level of theory.

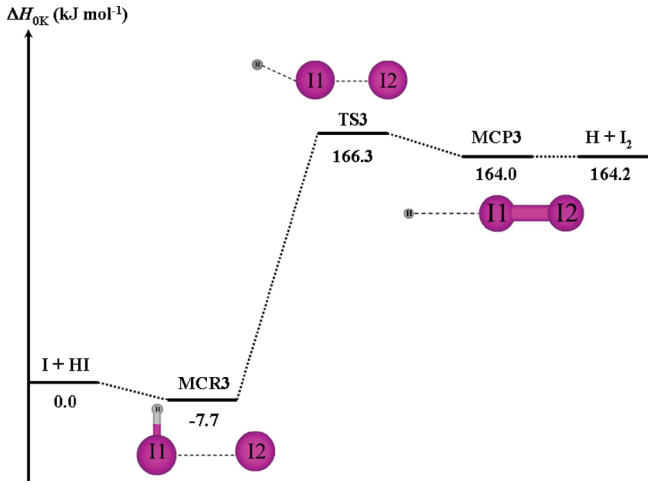

Figure 3. Potential energy profiles for the I ($^2P_{3/2}$) + HI reaction system calculated at the CCSD(T)/cc-pVTZ//MP2/cc-pVTZ level of theory.

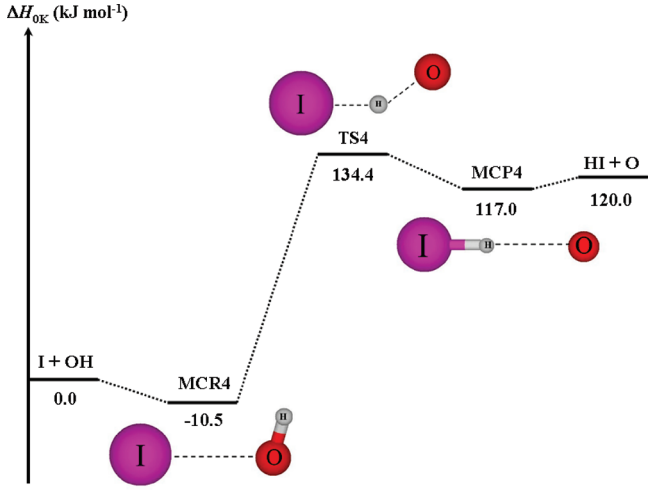

Figure 4. Potential energy profiles for the I ($^2P_{3/2}$) + OH reaction system calculated at the CCSD(T)/cc-pVTZ//MP2/cc-pVTZ level of theory.

reactions. Table 2 lists the essential structural parameters and imaginary vibrational frequencies calculated for the TSs and molecular complexes (MCR and MCP) at different levels of theory. More detailed information regarding optimized geometric parameters (reactants and products), vibrational frequencies (reactants, molecular complexes, TSs, and products), and literature enthalpies of formation at 0 K are presented in the Tables 2S−5S of the Supporting Information.

Geometric Parameters. *Transition States.* The transition state structure TS1 is characterized by the colinearity of the breaking H1−H2 bond and the nascent I−H1 bond, while the transition state structures TS2, TS3, and TS4 are not linear. The TS3 structure was not characterized with both DFT functionals employed in this work (MPW1K and BHandHLYP), although exhaustive searches have been performed. The unpaired electron on the iodine atom attacks the H1−H2 (reaction R_1), the H1−O (reaction R_2), the I1−I2 (reaction R_3), and the H−O (reaction R_4) σ-bonds, and the two electrons of the σ-bond become unpaired. The main change in the geometrical structure of the TS can be characterized by the *L* parameter, defined as the ratio of the increase in the length of the bond being broken and the elongation of the bond being formed.[55] This parameter provides a reliable measure of the reactant- or product-like character of the concomitant TS. Large *L* values correspond to product-like TSs, while smaller values correspond to reactant-like TSs. The calculated values of the *L* parameter for each studied reaction are given in the Table 2. These values are all greater than 1 for all levels of theory and all studied reactions. They become fairly constant between the cc-pVTZ and cc-pVQZ basis sets whatever the method (MP2, MPW1K, and BHandHLYP). Besides, the values of the *L* parameter decrease slightly when using the 6-311G(d,p) basis set compared to the ones obtained using the cc-pVnZ basis sets (n = T and Q). The TS structures are indeed product-like. This is in agreement with Hammond's postulate,[56] which predicts a product-like character for the TS when the reaction is endoergic and a reactant-like character with an exoergic reaction.

Molecular Complexes. The IRC calculations at each level of theory have revealed that the Minimum Energy Pathways connect the TSs to loosely bound complexes in the forward and backward directions.

Reaction R_1. TS1 is connected to the I···H_2 reactant complex (MCR1) and also to the H···HI product complex (MCP1). The structures of MCR1 and MCP1 are similar to that of TS1, with the characteristic difference that the emerging new bond I−H1 is much shorter in the TS than in the MCR1 complex (1.641 compared to 3.655 Å calculated at the MP2/cc-pVTZ level of theory, respectively), and the breaking bond H1−H2 is much shorter in the TS than that in the MCP1 complex (1.328 compared to 2.846 Å calculated at the MP2/cc-pVTZ level of theory, respectively). A significant basis set effect on the computed intermolecular distance (H1−H2 and I−H1) is observed with the MP2 method, while such behavior is not noticed with the two DFT functionals (MPW1K and BHandHLYP).

Reaction R_2. TS2 is connected to the I···H_2O reactant complex (MCR2) and also to the HI···OH product complex (MCP2). When the iodine atom approaches the water molecule, it forms an intermolecular bond I−O of 2.963 Å at the MP2/cc-pVTZ level of theory. The structure of MCR2 is not in the same configuration as TS2, although it is located on the MEP. On the product side, the structure of MCP2 has been determined with an intermolecular bond H1−O of 2.229 Å at the MP2/cc-pVTZ level of theory.

Reaction R_3. TS3 is connected to the I···IH reactant complex (MCR3) and also to the H···I_2 product complex (MCP3). The intermolecular bond length I1−I2 in MCR3 was estimated to be about 3.467 Å at the MP2/cc-pVTZ level of theory. Its structure prefigures that of the associated TS along the reaction path, although the bond angle HI1I2 is very different in the MCR3 and TS3 structures (87.2 and 161.6° calculated at the MP2/cc-pVTZ level of theory, respectively). The MCP3 structure is characterized by the near colinearity of the three atoms (H, I1, and I2) and an intermolecular bond length H−I1 of 3.436 Å at the MP2/cc-pVTZ level of theory.

Reaction R_4. TS4 is connected to the I···OH reactant complex (MCR4) and also to the IH···O product complex (MCP4). When the iodine atom approaches the hydroxyl radical on the triplet Potential Energy Surface, it forms an intermolecular bond I−O of 3.027 Å at the MP2/cc-pVTZ level of theory. The structure of MCR4 is not in the same configuration as TS4, although it is located on the MEP. On the product side, the structure of MCP4 has been determined with an intermolecular bond H−O of 2.515 Å at the MP2/cc-pVTZ level of theory.

Vibrational Frequencies. In all cases, the eigenvector in the TS corresponding to the imaginary frequency is primarily a motion of the atom being transferred. As seen in Table 2, the DFT imaginary frequencies are found to be considerably lower than those calculated by the MP2 method. Whatever the method

TABLE 2: Essential Structural Parameters[a] and Imaginary Frequencies for the TSs and Molecular Complexes of the Studied Reactions at Different Levels of Theory

I ($^2P_{3/2}$) + H_2 → HI + H (R_1)

		r(H1−H2)			*r*(I−H1)			*θ*(IH1H2)				
level of theory		MCR1	TS1	MCP1	MCR1	TS1	MCP1	MCR1	TS1	MCP1	L^b	$\nu^{\neq}$, cm^{-1}
MP2	cc-pVTZ	0.737	1.328	2.846	3.655	1.641	1.598	180.0	180.0	180.0	13.8	872i
	cc-pVQZ	0.737	1.325	2.518	3.524	1.631	1.590	180.0	180.0	180.0	13.9	836i
	6-311G(d,p)	0.739	1.286	3.291	3.857	1.663	1.606	180.0	180.0	180.0	9.5	1102i
MPW1K	cc-pVTZ	0.740	1.745	2.320	4.311	1.620	1.608	180.0	180.0	180.0	70.3	244i
	cc-pVQZ	0.739	1.737	1.984	4.311	1.618	1.609	180.0	180.0	180.0	66.8	253i
	6-311G(d,p)	0.741	1.641	2.144	4.256	1.633	1.615	180.0	180.0	180.0	43.2	351i
BHandHLYP	cc-pVTZ	0.737	1.889	1.991	3.996	1.616	1.613	180.0	180.0	180.0	122.5	111i
	cc-pVQZ	0.736	1.861	1.994	3.997	1.614	1.610	180.0	180.0	180.0	117.2	132i
	6-311G(d,p)	0.739	1.703	2.051	3.735	1.630	1.618	180.0	180.0	180.0	56.1	265i

I ($^2P_{3/2}$) + H_2O → HI + OH (R_2)

		r(H1−O)			*r*(I−H1)			*θ*(IH1O)			*ϕ*(IH1OH2)				
level of theory		MCR2	TS2	MCP2	MCR2	TS2	MCP2	MCR2	TS2	MCP2	MCR2	TS2	MCP2	L^b	$\nu^{\neq}$, cm^{-1}
MP2	cc-pVTZ	0.961	1.545	2.229	3.325	1.646	1.603	60.0	148.1	174.9	−108.1	−46.8	−3.6	12.4	539i
	cc-pVQZ	0.960	1.553	2.201	2.926	1.634	1.601	58.1	146.6	176.7	−111.3	−42.8	−3.8	13.3	511i
	6-311G(d,p)	0.960	1.481	2.281	3.413	1.673	1.610	57.5	148.3	174.9	−112.5	−51.4	−3.6	7.7	901i
MPW1K	cc-pVTZ	0.952	1.732	2.220	3.197	1.635	1.613	62.3	143.5	170.8	−104.4	−55.3	0.2	13.9	203i
	cc-pVQZ	0.952	1.730	2.235	3.228	1.633	1.610	61.7	142.2	171.7	−105.6	−52.4	0.1	13.9	231i
	6-311G(d,p)	0.953	1.620	2.133	3.183	1.657	1.622	60.1	143.4	172.9	−107.5	−59.0	0.0	9.2	386i
BHandHLYP	cc-pVTZ	0.951	1.599	2.268	3.307	1.653	1.612	60.0	149.0	172.2	−108.9	−45.4	1.2	14.1	429i
	cc-pVQZ	0.950	1.595	2.296	3.358	1.650	1.609	58.8	151.3	171.8	−111.4	−34.1	0.7	14.2	434i
	6-311G(d,p)	0.952	1.530	2.186	3.276	1.675	1.620	58.3	147.8	172.8	−111.3	−52.4	−10.4	9.4	655i

I ($^2P_{3/2}$) + HI → H + I_2 (R_3)

		r(I1−I2)			*r*(I1−H)			*θ*(HI1I2)				
level of theory		MCR3	TS3	MCP3	MCR3	TS3	MCP3	MCR3	TS3	MCP3	L^b	$\nu^{\neq}$, cm^{-1}
MP2	cc-pVTZ	3.467	2.656	2.658	1.599	2.331	3.436	87.2	161.6	179.9		634i
	cc-pVQZ	3.290	2.637	2.637	1.591	2.321	3.010	87.0	164.6	179.9	738.9	577i
	6-311G(d,p)	3.958	2.721	2.715	1.607	2.309	4.042	91.4	159.6	179.9	115.0	780i

I ($^2P_{3/2}$) + OH → HI + O (^3P) (R_4)

		r(O−H)			*r*(I−H)			*θ*(IOH)				
level of theory		MCR4	TS4	MCP4	MCR4	TS4	MCP4	MCR4	TS4	MCP4	L^b	$\nu^{\neq}$, cm^{-1}
MP2	cc-pVTZ	0.970	1.374	2.515	3.369	1.683	1.599	61.4	147.8	180.0	5.6	1549i
	cc-pVQZ	0.968	1.373	2.465	3.292	1.672	1.591	61.0	145.9	180.0	5.2	1494i
	6-311G(d,p)	0.968	1.351	2.574	3.470	1.708	1.606	60.2	147.0	180.0	4.5	1822i
MPW1K	cc-pVTZ	0.965	1.509	2.497	3.066	1.667	1.609	64.1	139.9	175.9	9.0	754i
	cc-pVQZ	0.964	1.507	2.519	3.059	1.665	1.606	63.6	140.6	175.8	8.8	761i
	6-311G(d,p)	0.966	1.469	2.384	3.090	1.686	1.615	62.0	137.1	179.4	6.8	940i
BHandHLYP	cc-pVTZ	0.964	1.453	2.490	3.232	1.685	1.609	62.5	147.9	179.3	6.3	1023i
	cc-pVQZ	0.963	1.451	2.509	3.264	1.682	1.606	61.4	150.0	179.3	6.3	1018i
	6-311G(d,p)	0.944	1.419	2.417	3.224	1.705	1.615	61.2	143.3	179.3	5.0	1263i

[a] Bond lengths *r* are in angstroms, and bond angles *θ* and dihedral angles *ϕ* are in degrees. [b] The parameter *L* is defined as the ratio of the increase in the length of the bond being broken and the elongation of the bond being formed, each with respect to its equilibrium value in the reactant and the product.

(MP2, MPW1K, and BHandHLYP), the values of the imaginary frequency are found to be larger with the 6-311G(d,p) basis set than the ones obtained with the cc-pVnZ basis sets (n = T and Q).

2. Energetics. Table 3 lists for the four studied reactions the reaction enthalpies $\Delta_r H$ at 0 K calculated at the different levels of theory. The results obtained indicate that the reactions are predicted to be endothermic. For each reaction, the $\Delta_r H$ values are very consistent when using the same single-point energy level of theory on the different geometries. For example, the computed $\Delta_r H(R_1)$ at 0 K are 139.0, 139.3, and 139.0 kJ mol^{-1} at the CCSD(T)/cc-pVTZ//MP2/cc-pVTZ, CCSD(T)/cc-pVTZ//MPW1K/cc-pVTZ, and CCSD(T)/cc-pVTZ//BHandHLYP/cc-pVTZ levels of theory, respectively. The highest differences in the computed values for the same single-point energy level of theory are 0.6, 1.6, 0.1, and 0.8 kJ mol^{-1} for the reactions R_1, R_2, R_3, and R_4, respectively. These results show that the computed reaction enthalpies do not depend on the geometry optimization level of theory. The basis set in the CCSD(T) single-point energy calculation does affect significantly the $\Delta_r H$ at 0 K values. Increasing the basis sets size from cc-pVTZ to cc-pV5Z changes the values by about 10, 2, 16, and 1 kJ mol^{-1} for the reactions R_1, R_2, R_3, and R_4, respectively. The same trends are observed when going from the aug-cc-pVTZ to the aug-cc-pV5Z basis sets. Adding more diffuse functions to the Dunning's basis sets tends to decrease the

TABLE 3: Reaction Enthalpies $\Delta_r H$ Calculated at 0 K in kJ mol^{-1} at Different Levels of Theory Including Spin−Orbit Corrections

I ($^2P_{3/2}$) + H_2 → HI + H (R_1)

	geometry optimization level of theory					
	MP2		MPW1K		BHandHLYP	
SPC level of theory	cc-pVTZ	cc-pVQZ	cc-pVTZ	cc-pVQZ	cc-pVTZ	cc-pVQZ
CCSD(T)/cc-pVTZ	139.0		139.3		139.0	
CCSD(T)/cc-pVQZ	131.5	131.8	131.8	131.9	131.6	131.6
CCSD(T)/cc-pV5Z	129.0	129.2	129.5	129.5	129.3	129.3
CCSD(T)/aug-cc-pVTZ	133.7		134.0		133.7	
CCSD(T)/aug-cc-pVQZ	125.7	126.0	126.1	126.2	125.9	125.9
CCSD(T)/aug-cc-pV5Z	122.1	122.1	122.7	122.6	122.5	122.4

	geometry optimization level of theory		
SPC level of theory	MP2/6-311G(d,p)	MPW1K/6-311G(d,p)	BHandHLYP/6-311G(d,p)
CCSD(T)/6-311G(d,p)	143.5	143.9	143.6
CCSD(T)/6-311+G(3df,2p)	139.9	140.4	139.9
CCSD(T)/6-311++G(3df,3pd)	133.2	133.7	133.3
experimental value (literature)		*137.4 ± 0.3*	

I ($^2P_{3/2}$) + H_2O → HI + OH (R_2)

	geometry optimization level of theory					
	MP2		MPW1K		BHandHLYP	
SPC level of theory	cc-pVTZ	cc-pVQZ	cc-pVTZ	cc-pVQZ	cc-pVTZ	cc-pVQZ
CCSD(T)/cc-pVTZ	189.4		188.2		188.0	
CCSD(T)/cc-pVQZ	188.0	188.4	187.0	186.9	186.9	186.8
CCSD(T)/cc-pV5Z	187.8	188.0	187.0	186.9	186.9	186.8
CCSD(T)/aug-cc-pVTZ	189.2		188.0		187.8	
CCSD(T)/aug-cc-pVQZ	184.5	184.9	183.6	183.4	183.4	183.3
CCSD(T)/aug-cc-pV5Z	181.5	181.6	180.8	180.6	180.6	180.5

	geometry optimization level of theory		
SPC level of theory	MP2/6-311G(d,p)	MPW1K/6-311G(d,p)	BHandHLYP/6-311G(d,p)
CCSD(T)/6-311G(d,p)	184.4	183.4	183.4
CCSD(T)/6-311+G(3df,2p)	194.9	194.5	194.2
CCSD(T)/6-311++G(3df,3pd)	190.7	190.2	190.0
experimental value (literature)		*198.7 ± 1.5*	

I ($^2P_{3/2}$) + HI → H + I_2 (R_3)

	geometry optimization level of theory	
	MP2	
SPC level of theory	cc-pVTZ	cc-pVQZ
CCSD(T)/cc-pVTZ	164.2	
CCSD(T)/cc-pVQZ	153.0	153.1
CCSD(T)/cc-pV5Z	148.3	148.2
CCSD(T)/aug-cc-pVTZ	162.2	
CCSD(T)/aug-cc-pVQZ	152.0	152.1
CCSD(T)/aug-cc-pV5Z	150.6	150.6

	geometry optimization level of theory
SPC level of theory	MP2/6-311G(d,p)
CCSD(T)/6-311G(d,p)	178.5
CCSD(T)/6-311+G(3df,2p)	149.2
CCSD(T)/6-311++G(3df,3pd)	160.3
experimental value (literature)	*145.8 ± 0.4*

I ($^2P_{3/2}$) + OH → HI + O (^3P) (R_4)

	geometry optimization level of theory					
	MP2		MPW1K		BHandHLYP	
SPC level of theory	cc-pVTZ	cc-pVQZ	cc-pVTZ	cc-pVQZ	cc-pVTZ	cc-pVQZ
CCSD(T)/cc-pVTZ	120.0		119.5		119.4	
CCSD(T)/cc-pVQZ	120.3	120.6	119.9	119.9	119.9	119.8
CCSD(T)/cc-pV5Z	120.6	120.7	120.4	120.3	120.3	120.2
CCSD(T)/aug-cc-pVTZ	121.4		120.8		120.8	
CCSD(T)/aug-cc-pVQZ	117.4	117.6	117.0	117.0	117.0	116.9
CCSD(T)/aug-cc-pV5Z	114.5	114.5	114.4	114.3	114.4	114.3

TABLE 3: Continued

SPC level of theory	geometry optimization level of theory		
	MP2/6-311G(d,p)	MPW1K/6-311G(d,p)	BHandHLYP/6-311G(d,p)
CCSD(T)/6-311G(d,p)	112.2	112.1	112.0
CCSD(T)/6-311+G(3df,2p)	127.2	127.2	126.8
CCSD(T)/6-311++G(3df,3pd)	124.3	124.2	124.0
experimental value (literature)		*129.8 ± 1.6*	

computed reaction enthalpies at 0 K. Important changes in the results are also noticed when using the Pople-type basis sets. Increasing the basis sets size from 6-311G(d,p) to 6-311+G(3df,2p) changes the values by about −4, +11, −29, and +15 kJ mol^{-1} for the reactions R_1, R_2, R_3, and R_4, respectively. Less marked trends are observed when going from the 6-311+G(3df,2p) to the 6-311++G(3df,3pd) basis sets (−7, −4, +11, and −3 kJ mol^{-1}).

The $\Delta_r H$ at 0 K values have been calculated using the literature heats of formation $\Delta_f H^0$ at 0 K for the species of interest (see Table 5S in the Supporting Information for data and relevant reference). Their values are also listed for each reaction in the Table 3. The calculated reaction enthalpies at the CCSD(T)/6-311+G(3df,2p) and CCSD(T)/6-311++G(3df,3pd) levels of theory are particularly in good agreement with their literature counterparts if the experimental uncertainties are taken into consideration. The difference is far more important between the computed $\Delta_r H$ at 0 K with the Dunning's basis sets and the corresponding literature values.

Table 4 shows for the reactions R_1, R_2, R_3, and R_4 the computed vibrationally adiabatic barriers at the different levels of theory. The H-abstraction from H_2, H_2O, and OH and the I-abstraction from HI appear to have a large electronic barrier. The computed vibrationally adiabatic barriers depend slightly on the geometry optimization level of theory when the same method is employed. For example, the $E_0(R_4)$ values are 131.1, and 131.7 kJ mol^{-1} at the CCSD(T)/cc-pVQZ//MP2/cc-pVTZ and CCSD(T)/cc-pVQZ//MP2/cc-pVQZ levels, respectively. Similar trends are observed with the MPW1K and BHandHLYP functionals. If we compare the results obtained using the same level of theory as that for the single-point energy calculation and different methods for the geometry optimization, it can be seen that the E_0's calculated at the CCSD(T)//MP2 levels are systematically lower by about 1 to 6 kJ mol^{-1} when compared to those obtained at the CCSD(T)//MPW1K levels. The barriers calculated at the CCSD(T)//BHandHLYP level are closer to those obtained at the CCSD(T)//MP2 level, but the E_0's are still slightly higher by about 1−3 kJ mol^{-1}. The vibrationally adiabatic barriers are very sensitive to the basis set employed in the CCSD(T) single-point energy calculation. Increasing the basis sets size either from cc-pVTZ to cc-pV5Z (cc-pVQZ for the reaction R_2) or from aug-cc-pVTZ to aug-cc-pV5Z (for the reactions R_1, R_3, and R_4) tends to decrease drastically the E_0 values. The same trends are observed when more diffuse functions are added to the Dunning's basis sets or when using the Pople-type basis sets. If we compare the results obtained using the CCSD(T)/6-311+G(3df,2p) and CCSD(T)/cc-pVTZ levels of theory, it can be seen that the E_0 values are close to each other and independent of the geometry level. The same trends are observed using the CCSD(T)/6-311++G(3df,3pd) and CCSD(T)/cc-pVQZ levels of theory.

Table 5 lists the relative enthalpies at 0 K for the prereactive and postreactive complexes at different levels of theory. It can be seen that the prereactive (MCR1) and postreactive (MCP1) complexes are not more stable than the reactants I + H_2 and HI + H, respectively ($\Delta H_{0K} < -2$ kJ mol^{-1}). For all other prereactive complexes (MCR2, MCR3, and MCR4), the stabilization energies at 0 K are in the range of −3 to −22 kJ mol^{-1}. Increasing the basis set size has little effect on the relative enthalpies of the prereactive complexes (MCR1, MCR2, and MCR4) and the postreactive complexes (MCP1, MCP2, MCP3, and MCP4), while it is not the case for the ΔH_{0K} of MCR3, where the change of the basis set from cc-pVTZ to aug-cc-pV5Z leads to decrease its value of about 15 kJ mol^{-1}.

3. Kinetic Parameters Calculations. ***Rate Constants.*** The calculations of the temperature dependence of rate constants have been performed at different levels of theory for the reaction of iodine atoms with H_2, H_2O, HI, and OH.

I ($^2P_{3/2}$) + H_2 → HI + H (R_1). Table 6 lists the rate constants calculated at 39 levels of theory for 6 different temperatures (300, 600, 1000, 1500, 2000, and 2500 K). A selection of literature values derived from experiments with the shock tube technique[10] and data evaluations[10,16] are also listed for comparison purposes. All other relevant literature values are given in Table 1. As presented in Table 6, the computed rate constants at 300 K range from 10^{-37} to 10^{-30} cm^3 molecule^{-1} s^{-1}, showing the strong dependence of the rate constant on the level of theory. The values of the rate constants calculated at 300 K at the CCSD(T)/cc-pVTZ//MP2/cc-pVTZ, CCSD(T)/cc-pVTZ//MPW1K/cc-pVTZ, and CCSD(T)/cc-pVTZ//BHandHLYP/cc-pVTZ levels of theory are 3.0×10^{-35}, 2.9×10^{-35}, and 6.6×10^{-35} cm^3 molecule^{-1} s^{-1}, respectively. They are in excellent agreement with the literature value at 300 K (8.5×10^{-35} cm^3 molecule^{-1} s^{-1}).[10] Similar results are obtained when using the CCSD(T) energies with the 6-311+G(3df,2p) basis set on MP2-, MPW1K-, and BHandHLYP-optimized geometries (6.6×10^{-35}, 8.7×10^{-35}, and 1.3×10^{-35} cm^3 molecule^{-1} s^{-1}). It can be noticed that the values computed at the CCSD(T)/cc-pVQZ and CCSD(T)/6-311++G(3df,3pd) levels of theory on MP2-optimized geometries are about 1 order of magnitude higher than the literature value. The calculated rate constants using CCSD(T) energies with the cc-pV5Z and aug-cc-pVnZ (n = T, Q, and 5) are 1−4 orders of magnitude higher than the literature value at 300 K. The differences between the calculated rate constants and their literature counterparts are however less and less marked as the temperature rises. We observe for examples at 2000 K a good agreement between the experimental value[10] of 8.8×10^{-14} cm^3 molecule^{-1} s^{-1} and our calculated values at the CCSD(T)/cc-pVTZ//MP2/cc-pVTZ and CCSD(T)/6-311++G(3df,2p)//MP2/6-311G(d,p) levels of theory (2.5×10^{-13} and 2.7×10^{-13} cm^3 molecule^{-1} s^{-1}, respectively). By comparison to the literature values over the whole temperature range (250−2500 K), the most appropriate levels of theory to compute quantitatively the temperature dependence of the rate constant are the CCSD(T)/cc-pVTZ//MP2/cc-pVTZ and CCSD(T)/6-311++G(3df,2p)//MP2/6-311G(d,p). In the same manner, semiquantitative results (difference of about 1 order of magnitude in the rate constant) are obtained when using the CCSD(T)/cc-pVQZ//MP2/cc-pVQZ and CCSD(T)/6-311++G(3df,3pd)//MP2/6-311G(d,p) levels of theory. Figure 5 presents

TABLE 4: Vibrationally Adiabatic Barriers E_0 Calculated in kJ mol^{-1} at Different Levels of Theory Including Spin−Orbit Corrections

$I\ (^2P_{3/2}) + H_2 \rightarrow HI + H\ (R_1)$

	geometry optimization level of theory					
	MP2		MPW1K		BHandHLYP	
SPC level of theory	cc-pVTZ	cc-pVQZ	cc-pVTZ	cc-pVQZ	cc-pVTZ	cc-pVQZ
CCSD(T)/cc-pVTZ	144.5		145.2		143.9	
CCSD(T)/cc-pVQZ	135.4	135.9	136.7	136.8	135.6	135.7
CCSD(T)/cc-pV5Z	132.5	132.9	134.6	134.6	133.4	133.5
CCSD(T)/aug-cc-pVTZ	134.4		136.1		135.2	
CCSD(T)/aug-cc-pVQZ	124.8	125.2	127.2	127.1	126.4	126.5
CCSD(T)/aug-cc-pV5Z	117.7	117.7	121.9	121.7	121.8	121.6

	geometry optimization level of theory		
SPC level of theory	MP2/6-311G(d,p)	MPW1K/6-311G(d,p)	BHandHLYP/6-311G(d,p)
CCSD(T)/6-311G(d,p)	154.6	155.3	154.2
CCSD(T)/6-311+G(3df,2p)	144.7	147.6	146.8
CCSD(T)/6-311++G(3df,3pd)	136.4	139.7	139.0

$I\ (^2P_{3/2}) + H_2O \rightarrow HI + OH\ (R_2)$

	geometry optimization level of theory					
	MP2		MPW1K		BHandHLYP	
SPC level of theory	cc-pVTZ	cc-pVQZ	cc-pVTZ	cc-pVQZ	cc-pVTZ	cc-pVQZ
CCSD(T)/cc-pVTZ	189.7		190.6		189.2	
CCSD(T)/cc-pVQZ	186.3	186.9	188.1	187.6	186.3	185.7
CCSD(T)/aug-cc-pVTZ	184.0		186.1		183.8	

	geometry optimization level of theory		
SPC level of theory	MP2/6-311G(d,p)	MPW1K/6-311G(d,p)	BHandHLYP/6-311G(d,p)
CCSD(T)/6-311G(d,p)	191.2	192.5	191.6
CCSD(T)/6-311+G(3df,2p)	192.2	197.0	194.1
CCSD(T)/6-311++G(3df,3pd)	186.6	192.2	188.9

$I\ (^2P_{3/2}) + HI \rightarrow H + I_2\ (R_3)$

	geometry optimization level of theory	
	MP2	
SPC level of theory	cc-pVTZ	cc-pVQZ
CCSD(T)/cc-pVTZ	166.3	
CCSD(T)/cc-pVQZ	151.1	152.1
CCSD(T)/cc-pV5Z	144.8	145.6
CCSD(T)/aug-cc-pVTZ	158.3	
CCSD(T)/aug-cc-pVQZ	146.0	147.1
CCSD(T)/aug-cc-pV5Z	143.6	144.5

SPC level of theory	geometry optimization level of theory MP2/6-311G(d,p)
CCSD(T)/6-311G(d,p)	187.5
CCSD(T)/6-311+G(3df,2p)	150.2
CCSD(T)/6-311++G(3df,3pd)	158.4

$I\ (^2P_{3/2}) + OH \rightarrow HI + O\ (^3P)\ (R_4)$

	geometry optimization level of theory					
	MP2		MPW1K		BHandHLYP	
SPC level of theory	cc-pVTZ	cc-pVQZ	cc-pVTZ	cc-pVQZ	cc-pVTZ	cc-pVQZ
CCSD(T)/cc-pVTZ	134.4		137.6		136.1	
CCSD(T)/cc-pVQZ	131.1	131.7	135.0	134.9	133.6	133.4
CCSD(T)/cc-pV5Z	130.5	130.9	134.8	134.6	133.4	133.2
CCSD(T)/aug-cc-pVTZ	127.5		131.9		130.0	
CCSD(T)/aug-cc-pVQZ	121.2	121.8	126.4	126.1	124.2	123.8
CCSD(T)/aug-cc-pV5Z	118.7	119.2	124.2	123.9	121.9	121.3

	geometry optimization level of theory		
SPC level of theory	MP2/6-311G(d,p)	MPW1K/6-311G(d,p)	BHandHLYP/6-311G(d,p)
CCSD(T)/6-311G(d,p)	138.6	141.1	139.9
CCSD(T)/6-311+G(3df,2p)	137.6	143.3	140.8
CCSD(T)/6-311++G(3df,3pd)	132.2	138.5	135.8

TABLE 5: Relative Enthalpies at 0 K in kJ mol^{-1} for the Pre-Reactive and Post-Reactive Complexes at Different Levels of Theory Including Spin−Orbit Corrections[a]

I ($^2P_{3/2}$) + H_2 → HI + H (R_1)

	geometry optimization level of theory											
	MP2				MPW1K				BHandHLYP			
	cc-pVTZ		cc-pVQZ		cc-pVTZ		cc-pVQZ		cc-pVTZ		cc-pVQZ	
SPC level of theory	MCR1	MCP1	MCR1	MCP1	MCR1	MCP1	MCR1	MCP1	MCR1	MCP1	MCR1	MCP1
CCSD(T)/cc-pVTZ	0.4	139.5 (0.5)			0.0	140.6 (1.3)			0.2	141.4 (2.4)		
CCSD(T)/cc-pVQZ	0.1	131.8 (0.3)	0.9	132.7 (0.9)	−0.1	132.5 (0.7)	0.0	133.3 (1.4)	0.0	133.1 (1.5)	0.0	133.2 (1.6)
CCSD(T)/cc-pV5Z	−0.1	129.2 (0.2)	0.6	129.9 (0.9)	−0.1	130.2 (0.7)	−0.1	131.0 (1.5)	−0.1	130.9 (1.6)	0.0	130.9 (1.6)
CCSD(T)/aug-cc-pVTZ	−1.5	132.8 (−0.9)			−1.1	132.8 (−1.2)			−1.2	132.9 (−0.9)		
CCSD(T)/aug-cc-pVQZ	−1.8	124.8 (−0.9)	−1.2	125.2 (−0.8)	−1.2	124.8 (−1.3)	−1.1	124.5 (−1.7)	−1.4	124.4 (−1.5)	−1.4	124.4 (−1.5)
CCSD(T)/aug-cc-pV5Z	−1.6	121.4 (−0.7)	−0.9	121.5 (−0.6)	−1.1	121.3 (−1.4)	−1.0	120.0 (−2.6)	−1.2	120.1 (−2.4)	−1.2	120.0 (−2.4)

	geometry optimization level of theory					
	MP2/6-311G(d,p)		MPW1K/6-311G(d,p)		BHandHLYP/6-311G(d,p)	
SPC level of theory	MCR1	MCP1	MCR1	MCP1	MCR1	MCP1
CCSD(T)/6-311G(d,p)	1.1	143.9 (0.4)	0.1	148.3 (4.4)	1.1	148.7 (5.1)
CCSD(T)/6-311+G(3df,2p)	0.8	140.1 (0.2)	−0.1	142.8 (2.4)	0.8	142.9 (3.0)
CCSD(T)/6-311++G(3df,3pd)	0.3	133.1 (0.1)	−0.4	135.2 (1.5)	0.1	135.3 (2.0)

I ($^2P_{3/2}$) + H_2O → HI + OH (R_2)

	geometry optimization level of theory											
	MP2				MPW1K				BHandHLYP			
	cc-pVTZ		cc-pVQZ		cc-pVTZ		cc-pVQZ		cc-pVTZ		cc-pVQZ	
SPC level of theory	MCR2	MCP2	MCR2	MCP2	MCR2	MCP2	MCR2	MCP2	MCR2	MCP2	MCR2	MCP2
CCSD(T)/cc-pVTZ	−13.2	183.1 (−6.3)			−12.2	181.8 (−6.4)			−13.0	181.4 (−6.6)		
CCSD(T)/cc-pVQZ	−13.4	182.4 (−5.6)	−13.7	183.3 (−5.1)	−12.6	181.4 (−5.6)	−12.9	181.1 (−5.8)	−13.1	181.1 (−5.8)	−13.3	180.8 (−6.0)
CCSD(T)/aug-cc-pVTZ	−13.7	181.8 (−7.4)			−12.7	180.5 (−7.5)			−13.4	180.2 (−7.6)		

	geometry optimization level of theory					
	MP2/6-311G(d,p)		MPW1K/6-311G(d,p)		BHandHLYP/6-311G(d,p)	
SPC level of theory	MCR2	MCP2	MCR2	MCP2	MCR2	MCP2
CCSD(T)/6-311G(d,p)	−14.2	176.4 (−8.0)	−11.3	176.9 (−6.5)	−12.6	175.7 (−7.5)
CCSD(T)/6-311+G(3df,2p)	−11.2	189.6 (−5.3)	−8.8	190.1 (−4.4)	−9.7	189.0 (−5.2)
CCSD(T)/6-311++G(3df,3pd)	−10.9	185.0 (−5.7)	−8.5	185.6 (−4.6)	−9.5	184.5 (−5.5)

I ($^2P_{3/2}$) + HI → H + I_2 (R_3)

	geometry optimization level of theory			
	MP2			
	cc-pVTZ		cc-pVQZ	
SPC level of theory	MCR3	MCP3	MCR3	MCP3
CCSD(T)/cc-pVTZ	−7.7	164.0 (−0.2)		
CCSD(T)/cc-pVQZ	−15.3	152.0 (−1.0)	−15.1	151.8 (−1.3)
CCSD(T)/cc-pV5Z	−17.8	146.7 (−1.6)	−17.7	145.9 (−2.3)
CCSD(T)/aug-cc-pVTZ	−16.0	159.6 (−2.6)		
CCSD(T)/aug-cc-pVQZ	−20.9	148.8 (−3.2)	−21.3	147.9 (−4.2)
CCSD(T)/aug-cc-pV5Z	−21.9	147.2 (−3.4)	−22.3	146.1 (−4.5)

	geometry optimization level of theory	
	MP2/6-311G(d,p)	
SPC level of theory	MCR3	MCP3
CCSD(T)/6-311G(d,p)	−3.4	178.7 (0.2)
CCSD(T)/6-311+G(3df,2p)	−8.2	149.0 (0.2)
CCSD(T)/6-311++G(3df,3pd)	−8.2	159.8 (−0.5)

TABLE 5: Continued

I ($^2P_{3/2}$) + OH → HI + O (^3P) (R_4)

	geometry optimization level of theory											
	MP2				MPW1K				BHandHLYP			
	cc-pVTZ		cc-pVQZ		cc-pVTZ		cc-pVQZ		cc-pVTZ		cc-pVQZ	
SPC level of theory	MCR4	MCP4	MCR4	MCP4	MCR4	MCP4	MCR4	MCP4	MCR4	MCP4	MCR4	MCP4
CCSD(T)/cc-pVTZ	−10.5	117.0 (−3.0)			−9.5	115.7 (−3.8)			−10.2	115.6 (−3.8)		
CCSD(T)/cc-pVQZ	−11.1	117.6 (−2.7)	−11.6	118.0 (−2.6)	−11.4	116.6 (−3.3)	−11.5	116.4 (−3.5)	−11.3	116.4 (−3.5)	−11.3	116.3 (−3.5)
CCSD(T)/cc-pV5Z	−11.5	118.4 (−2.4)	−12.1	118.5 (−2.2)	−10.6	117.4 (−3.0)	−12.4	117.2 (−3.1)	−11.9	117.3 (−3.0)	−11.8	117.1 (−3.1)
CCSD(T)/aug-cc-pVTZ	−12.2	117.0 (−4.4)			−12.7	115.7 (−5.1)			−12.4	115.5 (−5.3)		
CCSD(T)/aug-cc-pVQZ	−14.8	111.6 (−5.8)	−15.5	111.7 (−5.9)	−16.0	110.5 (−6.5)	−14.9	111.7 (−6.3)	−15.3	110.3 (−6.7)	−13.9	111.6 (−5.3)
CCSD(T)/aug-cc-pV5Z	−8.8	110.5 (−4.0)	−14.2	110.4 (−4.1)	−13.8	109.7 (−4.7)	−14.8	109.5 (−4.8)	−14.0	109.5 (−4.9)	−13.9	109.3 (−5.0)

	geometry optimization level of theory					
	MP2/6-311G(d,p)		MPW1K/6-311G(d,p)		BHandHLYP/6-311G(d,p)	
SPC level of theory	MCR4	MCP4	MCR4	MCP4	MCR4	MCP4
CCSD(T)/6-311G(d,p)	−10.9	107.9 (−4.3)	−8.7	107.7 (−4.4)	−9.9	107.5 (−4.5)
CCSD(T)/6-311+G(3df,2p)	−9.5	124.5 (−2.7)	−9.2	123.5 (−3.7)	−9.4	123.5 (−3.3)
CCSD(T)/6-311++G(3df,3pd)	−9.3	120.6 (−3.7)	−9.1	119.6 (−4.6)	−9.2	119.6 (−4.4)

[a] Values in parentheses correspond to the relative enthalpies at 0 K in kJ mol^{-1} with respect to the products.

TABLE 6: Calculated Rate Constants at Different Temperatures in cm^3 molecule^{-1} s^{-1} at Different Levels of Theory for the Reaction I ($^2P_{3/2}$) + H_2 → HI + H (R_1) and a Comparison with Literature Data

	temperature (K)					
SPC level of theory	300	600	1000	1500	2000	2500
CCSD(T)/cc-pVTZ//MP2/cc-pVTZ	3.0×10^{-35}	1.0×10^{-22}	1.6×10^{-17}	8.9×10^{-15}	2.5×10^{-13}	2.0×10^{-12}
CCSD(T)/cc-pVQZ//MP2/cc-pVTZ	1.2×10^{-33}	6.5×10^{-22}	4.9×10^{-17}	1.8×10^{-14}	4.3×10^{-13}	3.1×10^{-12}
CCSD(T)/cc-pV5Z//MP2/cc-pVTZ	3.7×10^{-33}	1.1×10^{-21}	6.9×10^{-17}	2.3×10^{-14}	5.1×10^{-13}	3.5×10^{-12}
CCSD(T)/aug-cc-pVTZ//MP2/cc-pVTZ	1.7×10^{-33}	7.9×10^{-22}	5.5×10^{-17}	2.0×10^{-14}	4.5×10^{-13}	3.2×10^{-12}
CCSD(T)/aug-cc-pVQZ//MP2/cc-pVTZ	8.2×10^{-32}	5.5×10^{-21}	1.8×10^{-16}	4.3×10^{-14}	8.1×10^{-13}	5.2×10^{-12}
CCSD(T)/aug-cc-pV5Z//MP2/cc-pVTZ	1.4×10^{-30}	2.3×10^{-20}	4.2×10^{-16}	7.7×10^{-14}	1.2×10^{-12}	7.3×10^{-12}
CCSD(T)/cc-pVQZ//MP2/cc-pVQZ	9.4×10^{-34}	5.9×10^{-22}	4.7×10^{-17}	1.8×10^{-14}	4.2×10^{-13}	3.1×10^{-12}
CCSD(T)/cc-pV5Z//MP2/cc-pVQZ	3.1×10^{-33}	1.1×10^{-21}	6.8×10^{-17}	2.3×10^{-14}	5.1×10^{-13}	3.6×10^{-12}
CCSD(T)/aug-cc-pVQZ//MP2/cc-pVQZ	6.9×10^{-32}	5.1×10^{-21}	1.7×10^{-16}	4.3×10^{-14}	8.0×10^{-13}	5.1×10^{-12}
CCSD(T)/aug-cc-pV5Z//MP2/cc-pVQZ	1.4×10^{-30}	2.3×10^{-20}	4.2×10^{-16}	7.8×10^{-14}	1.3×10^{-12}	7.4×10^{-12}
CCSD(T)/6-311G(d,p)//MP2/6-311G(d,p)	6.5×10^{-37}	1.5×10^{-23}	5.0×10^{-18}	4.0×10^{-15}	1.4×10^{-13}	1.3×10^{-12}
CCSD(T)/6-311+G(3df,2p)//MP2/6-311G(d,p)	6.6×10^{-35}	1.5×10^{-22}	2.0×10^{-17}	1.0×10^{-14}	2.7×10^{-13}	2.2×10^{-12}
CCSD(T)/6-311++G(3df,3pd)//MP2/6-311G(d,p)	9.4×10^{-34}	5.6×10^{-22}	4.4×10^{-17}	1.7×10^{-14}	4.1×10^{-13}	3.0×10^{-12}
CCSD(T)/cc-pVTZ//MPW1K/cc-pVTZ	2.9×10^{-35}	2.2×10^{-22}	4.6×10^{-17}	2.8×10^{-14}	8.1×10^{-13}	6.7×10^{-12}
CCSD(T)/cc-pVQZ//MPW1K/cc-pVTZ	8.9×10^{-34}	1.2×10^{-21}	1.3×10^{-16}	5.5×10^{-14}	1.3×10^{-12}	1.0×10^{-11}
CCSD(T)/cc-pV5Z//MPW1K/cc-pVTZ	2.1×10^{-33}	1.9×10^{-21}	1.7×10^{-16}	6.6×10^{-14}	1.5×10^{-12}	1.1×10^{-11}
CCSD(T)/aug-cc-pVTZ//MPW1K/cc-pVTZ	1.1×10^{-33}	1.4×10^{-21}	1.4×10^{-16}	5.8×10^{-14}	1.4×10^{-12}	1.0×10^{-11}
CCSD(T)/aug-cc-pVQZ//MPW1K/cc-pVTZ	4.1×10^{-32}	8.3×10^{-21}	4.1×10^{-16}	1.2×10^{-13}	2.4×10^{-12}	1.6×10^{-11}
CCSD(T)/aug-cc-pV5Z//MPW1K/cc-pVTZ	3.4×10^{-31}	2.4×10^{-20}	7.7×10^{-16}	1.8×10^{-13}	3.3×10^{-12}	2.1×10^{-11}
CCSD(T)/cc-pVQZ//MPW1K/cc-pVQZ	8.8×10^{-34}	1.2×10^{-21}	1.3×10^{-16}	5.5×10^{-14}	1.3×10^{-12}	1.0×10^{-11}
CCSD(T)/cc-pV5Z//MPW1K/cc-pVQZ	2.1×10^{-33}	1.9×10^{-21}	1.7×10^{-16}	6.6×10^{-14}	1.5×10^{-12}	1.1×10^{-11}
CCSD(T)/aug-cc-pVQZ//MPW1K/cc-pVQZ	4.1×10^{-32}	8.3×10^{-21}	4.1×10^{-16}	1.2×10^{-13}	2.4×10^{-12}	1.6×10^{-11}
CCSD(T)/aug-cc-pV5Z//MPW1K/cc-pVQZ	3.6×10^{-31}	2.5×10^{-20}	7.8×10^{-16}	1.8×10^{-13}	3.3×10^{-12}	2.1×10^{-11}
CCSD(T)/6-311G(d,p)//MPW1K/6-311G(d,p)	3.9×10^{-37}	1.9×10^{-23}	8.6×10^{-18}	7.6×10^{-15}	2.7×10^{-13}	2.5×10^{-12}
CCSD(T)/6-311+G(3df,2p)//MPW1K/6-311G(d,p)	8.7×10^{-35}	9.1×10^{-23}	2.2×10^{-17}	1.4×10^{-14}	4.2×10^{-13}	3.6×10^{-12}
CCSD(T)/6-311++G(3df,3pd)//MPW1K/6-311G(d,p)	2.1×10^{-34}	4.4×10^{-22}	5.6×10^{-17}	2.6×10^{-14}	6.8×10^{-13}	5.2×10^{-12}
CCSD(T)/cc-pVTZ//BHandHLYP/cc-pVTZ	6.6×10^{-35}	4.3×10^{-22}	8.4×10^{-17}	4.9×10^{-14}	1.4×10^{-12}	1.1×10^{-11}
CCSD(T)/cc-pVQZ//BHandHLYP/cc-pVTZ	1.9×10^{-33}	2.3×10^{-21}	2.3×10^{-16}	9.6×10^{-14}	2.3×10^{-12}	1.7×10^{-11}
CCSD(T)/cc-pV5Z//BHandHLYP/cc-pVTZ	4.5×10^{-33}	3.6×10^{-21}	3.0×10^{-16}	1.1×10^{-13}	2.6×10^{-12}	1.9×10^{-11}
CCSD(T)/aug-cc-pVTZ//BHandHLYP/cc-pVTZ	2.2×10^{-33}	2.5×10^{-21}	2.4×10^{-16}	2.0×10^{-13}	4.0×10^{-12}	2.7×10^{-11}
CCSD(T)/aug-cc-pVQZ//BHandHLYP/cc-pVTZ	7.3×10^{-32}	1.4×10^{-20}	6.9×10^{-16}	1.2×10^{-13}	2.4×10^{-12}	1.6×10^{-11}
CCSD(T)/aug-cc-pV5Z//BHandHLYP/cc-pVTZ	4.7×10^{-31}	3.7×10^{-20}	1.2×10^{-15}	2.9×10^{-13}	5.3×10^{-12}	3.3×10^{-11}
CCSD(T)/cc-pVQZ//BHandHLYP/cc-pVQZ	1.7×10^{-33}	2.1×10^{-21}	2.1×10^{-16}	8.7×10^{-14}	2.1×10^{-12}	1.6×10^{-11}
CCSD(T)/cc-pV5Z//BHandHLYP/cc-pVQZ	4.1×10^{-33}	3.2×10^{-21}	2.7×10^{-16}	1.0×10^{-13}	2.4×10^{-12}	1.7×10^{-11}
CCSD(T)/aug-cc-pVQZ//BHandHLYP/cc-pVQZ	6.8×10^{-32}	1.3×10^{-20}	6.3×10^{-16}	1.8×10^{-13}	3.7×10^{-12}	2.4×10^{-11}
CCSD(T)/aug-cc-pV5Z//BHandHLYP/cc-pVQZ	4.7×10^{-31}	3.5×10^{-20}	1.1×10^{-15}	2.7×10^{-13}	4.9×10^{-12}	3.1×10^{-11}
CCSD(T)/6-311G(d,p)//BHandHLYP/6-311G(d,p)	6.7×10^{-37}	2.8×10^{-23}	1.2×10^{-17}	1.0×10^{-14}	3.5×10^{-13}	3.2×10^{-12}
CCSD(T)/6-311+G(3df,2p)//BHandHLYP/6-311G(d,p)	1.3×10^{-35}	1.3×10^{-22}	2.9×10^{-17}	1.8×10^{-14}	5.4×10^{-13}	4.6×10^{-12}
CCSD(T)/6-311++G(3df,3pd)//BHandHLYP/6-311G(d,p)	3.0×10^{-34}	6.0×10^{-22}	7.3×10^{-17}	3.4×10^{-14}	8.7×10^{-13}	6.6×10^{-12}
Michael et al., 2000 [ref 10, *experiment*]					*8.8 × 10^{-14}*	*7.5 × 10^{-13}*
Michael et al., 2000 [ref 10, *evaluation*]	*8.5 × 10^{-35}*	*2.0 × 10^{-22}*	*1.2 × 10^{-17}*	*5.1 × 10^{-15}*	*8.8 × 10^{-14}*	*4.9 × 10^{-13}*
Baulch et al., 1981 [ref 16, *evaluation]*		*1.5 × 10^{-22}*	*1.7 × 10^{-17}*			

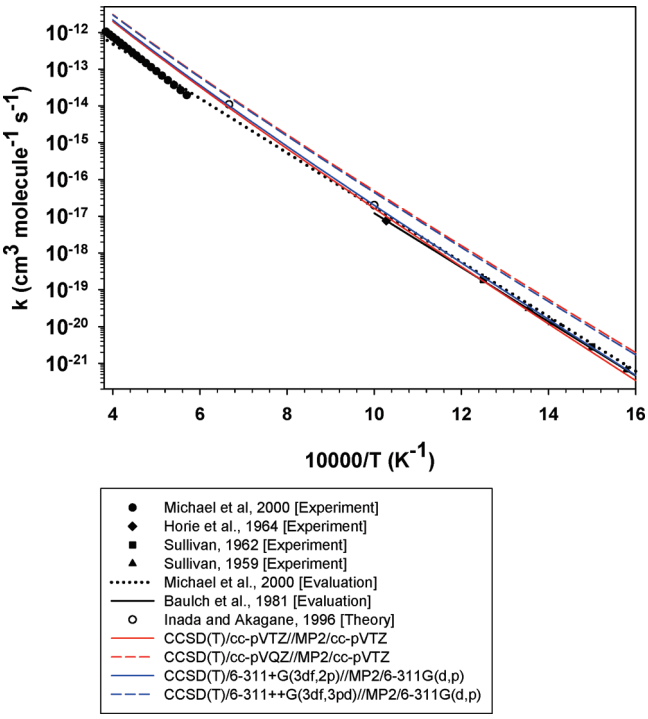

Figure 5. Temperature dependence of the rate constant of the reaction $I\ (^2P_{3/2}) + H_2 \rightarrow HI + H\ (R_1)$. Comparison with available literature data.

the results of the rate constant calculations at these four levels of theory together with the available literature data for comparison purposes. In order to make the plot readable, the temperature range was restrained to 625−2500 K. The results shown in Figure 5 and Table 6 indicate that our calculated values are in very good agreement with the experimental data of Michael et al.,[10] Horie et al.,[13] and Sullivan,[14,15] as well as with the ones reported by Baulch and co-workers in their review.[16] We observe at 1000 and 1500 K a very good agreement between the calculated values obtained by Inada and Akagane[11] (2.0×10^{-17} and 1.1×10^{-14} cm^3 molecule^{-1} s^{-1}, respectively) and our calculated values at the CCSD(T)/cc-pVnZ//MP2/cc-pVTZ (n = T and Q), CCSD(T)/6-311+G(3df,2p)//MP2/6-311G(d,p), and CCSD(T)/6-311++G(3df,3pd)//MP2/6-311G(d,p) levels of theory.

HI + H → I ($^2P_{3/2}$) + H_2 (R_{-1}). Table 7 lists the rate constants calculated at 39 levels of theory for 4 different temperatures (250, 300, 600, and 1000 K), together with the available literature values.[16−19] As shown in Table 7, the computed rate constants range from 10^{-13} to 10^{-10} cm^3 molecule^{-1} s^{-1} at 300 K. It is worth noticing that the differences at all temperatures between the computed rate constants and their literature counterparts are far less than an order of magnitude for 34 levels of theory. In particular, the values of the rate constants at 300 K calculated at the CCSD(T)/cc-pVnZ//MP2/cc-pVTZ (n = T and Q), CCSD(T)/6-311+G(3df,2p)//MP2/6-311G(d,p), and CCSD(T)/6-311++G(3df,3pd)//MP2/6-

TABLE 7: Calculated Rate Constants at Different Temperatures in cm^3 molecule^{-1} s^{-1} at Different Levels of Theory for the Reaction HI + H → I ($^2P_{3/2}$) + H_2 (R_{-1}) and a Comparison with Literature Data

	temperature (K)			
SPC level of theory	250	300	600	1000
CCSD(T)/cc-pVTZ//MP2/cc-pVTZ	5.5×10^{-12}	7.3×10^{-12}	2.0×10^{-11}	4.4×10^{-11}
CCSD(T)/cc-pVQZ//MP2/cc-pVTZ	1.2×10^{-11}	1.4×10^{-11}	2.7×10^{-11}	5.2×10^{-11}
CCSD(T)/cc-pV5Z//MP2/cc-pVTZ	1.4×10^{-11}	1.6×10^{-11}	2.9×10^{-11}	5.5×10^{-11}
CCSD(T)/aug-cc-pVTZ//MP2/cc-pVTZ	5.4×10^{-11}	4.9×10^{-11}	5.1×10^{-11}	7.7×10^{-11}
CCSD(T)/aug-cc-pVQZ//MP2/cc-pVTZ	1.2×10^{-10}	9.6×10^{-11}	7.2×10^{-11}	9.4×10^{-11}
CCSD(T)/aug-cc-pV5Z//MP2/cc-pVTZ	6.5×10^{-10}	3.9×10^{-10}	1.4×10^{-10}	1.4×10^{-10}
CCSD(T)/cc-pVQZ//MP2/cc-pVQZ	1.1×10^{-11}	1.3×10^{-11}	2.7×10^{-11}	5.3×10^{-11}
CCSD(T)/cc-pV5Z//MP2/cc-pVQZ	1.3×10^{-11}	1.5×10^{-11}	2.9×10^{-11}	5.6×10^{-11}
CCSD(T)/aug-cc-pVQZ//MP2/cc-pVQZ	1.1×10^{-10}	9.1×10^{-11}	7.2×10^{-11}	9.6×10^{-11}
CCSD(T)/aug-cc-pV5Z//MP2/cc-pVQZ	6.4×10^{-10}	3.8×10^{-10}	1.5×10^{-10}	1.5×10^{-10}
CCSD(T)/6-311G(d,p)//MP2/6-311G(d,p)	4.7×10^{-13}	9.3×10^{-13}	6.8×10^{-12}	2.2×10^{-11}
CCSD(T)/6-311+G(3df,2p)//MP2/6-311G(d,p)	9.6×10^{-12}	1.1×10^{-11}	2.4×10^{-11}	4.8×10^{-11}
CCSD(T)/6-311++G(3df,3pd)//MP2/6-311G(d,p)	2.1×10^{-11}	2.2×10^{-11}	3.3×10^{-11}	5.8×10^{-11}
CCSD(T)/cc-pVTZ//MPW1K/cc-pVTZ	4.4×10^{-12}	7.7×10^{-12}	4.4×10^{-11}	1.2×10^{-10}
CCSD(T)/cc-pVQZ//MPW1K/cc-pVTZ	7.5×10^{-12}	1.2×10^{-11}	5.5×10^{-11}	1.4×10^{-10}
CCSD(T)/cc-pV5Z//MPW1K/cc-pVTZ	6.9×10^{-12}	1.1×10^{-11}	5.3×10^{-11}	1.4×10^{-10}
CCSD(T)/aug-cc-pVTZ//MPW1K/cc-pVTZ	2.8×10^{-11}	3.5×10^{-11}	9.4×10^{-11}	2.0×10^{-10}
CCSD(T)/aug-cc-pVQZ//MPW1K/cc-pVTZ	4.8×10^{-11}	5.6×10^{-11}	1.2×10^{-10}	2.3×10^{-10}
CCSD(T)/aug-cc-pV5Z//MPW1K/cc-pVTZ	1.2×10^{-10}	1.2×10^{-10}	1.7×10^{-10}	2.8×10^{-10}
CCSD(T)/cc-pVQZ//MPW1K/cc-pVQZ	7.5×10^{-12}	1.2×10^{-11}	5.5×10^{-11}	1.4×10^{-10}
CCSD(T)/cc-pV5Z//MPW1K/cc-pVQZ	6.9×10^{-12}	1.1×10^{-11}	5.3×10^{-11}	1.4×10^{-10}
CCSD(T)/aug-cc-pVQZ//MPW1K/cc-pVQZ	4.9×10^{-11}	5.7×10^{-11}	1.2×10^{-10}	2.3×10^{-10}
CCSD(T)/aug-cc-pV5Z//MPW1K/cc-pVQZ	1.2×10^{-10}	1.2×10^{-10}	1.8×10^{-10}	2.9×10^{-10}
CCSD(T)/6-311G(d,p)//MPW1K/6-311G(d,p)	2.6×10^{-13}	6.6×10^{-13}	9.6×10^{-12}	4.0×10^{-11}
CCSD(T)/6-311+G(3df,2p)//MPW1K/6-311G(d,p)	2.0×10^{-12}	3.6×10^{-11}	2.3×10^{-11}	6.7×10^{-11}
CCSD(T)/6-311++G(3df,3pd)//MPW1K/6-311G(d,p)	3.5×10^{-12}	5.8×10^{-12}	2.9×10^{-11}	7.7×10^{-11}
CCSD(T)/cc-pVTZ//BHandHLYP/cc-pVTZ	9.3×10^{-12}	1.6×10^{-11}	8.0×10^{-11}	2.2×10^{-10}
CCSD(T)/cc-pVQZ//BHandHLYP/cc-pVTZ	1.5×10^{-11}	2.3×10^{-11}	9.7×10^{-11}	2.5×10^{-10}
CCSD(T)/cc-pV5Z//BHandHLYP/cc-pVTZ	1.4×10^{-11}	2.2×10^{-11}	9.5×10^{-11}	2.4×10^{-10}
CCSD(T)/aug-cc-pVTZ//BHandHLYP/cc-pVTZ	4.9×10^{-11}	6.2×10^{-11}	1.6×10^{-10}	3.3×10^{-10}
CCSD(T)/aug-cc-pVQZ//BHandHLYP/cc-pVTZ	7.7×10^{-11}	9.1×10^{-11}	1.9×10^{-10}	3.7×10^{-10}
CCSD(T)/aug-cc-pV5Z//BHandHLYP/cc-pVTZ	1.4×10^{-10}	1.5×10^{-10}	2.5×10^{-10}	4.3×10^{-10}
CCSD(T)/cc-pVQZ//BHandHLYP/cc-pVQZ	1.3×10^{-11}	2.0×10^{-11}	8.7×10^{-11}	2.2×10^{-10}
CCSD(T)/cc-pV5Z//BHandHLYP/cc-pVQZ	1.2×10^{-11}	1.9×10^{-11}	8.5×10^{-11}	2.2×10^{-10}
CCSD(T)/aug-cc-pVQZ//BHandHLYP/cc-pVQZ	7.1×10^{-11}	8.4×10^{-11}	1.8×10^{-10}	3.4×10^{-10}
CCSD(T)/aug-cc-pV5Z//BHandHLYP/cc-pVQZ	1.4×10^{-10}	1.5×10^{-10}	2.3×10^{-10}	4.0×10^{-10}
CCSD(T)/6-311G(d,p)//BHandHLYP/6-311G(d,p)	4.1×10^{-13}	1.0×10^{-12}	1.3×10^{-11}	5.3×10^{-11}
CCSD(T)/6-311+G(3df,2p)//BHandHLYP/6-311G(d,p)	2.4×10^{-12}	4.3×10^{-12}	2.8×10^{-11}	8.3×10^{-11}
CCSD(T)/6-311++G(3df,3pd)//BHandHLYP/6-311G(d,p)	4.3×10^{-12}	7.1×10^{-12}	3.5×10^{-11}	9.6×10^{-11}
Vasileiadis and Benson, 1997 [ref 17, *experiment*]		*2.1 × 10^{-11}*		
Umemoto et al., 1988 [ref 18, *experiment*]	*1.4 × 10^{-11}*	*1.8 × 10^{-11}*		
Lorenz et al., 1979 [ref 19, *experiment*]	*2.3 × 10^{-11}*	*2.8 × 10^{-11}*		
Baulch et al., 1981 [ref 16, *evaluation*]			*4.5 × 10^{-11}*	*5.7 × 10^{-11}*

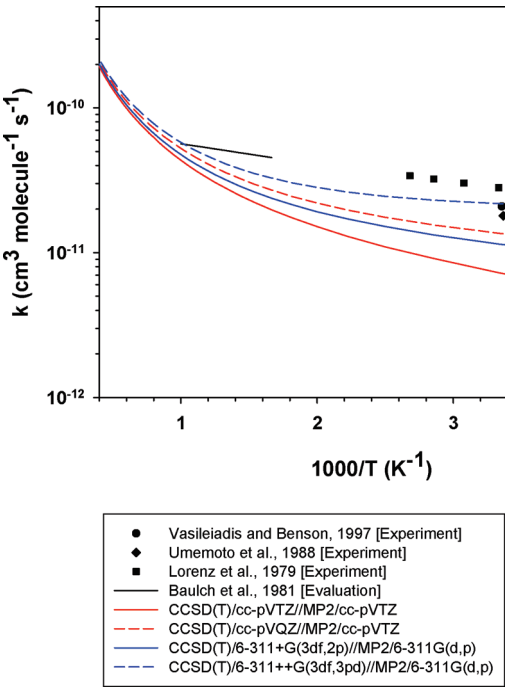

Figure 6. Temperature dependence of the rate constant of the reaction HI + H → I ($^2P_{3/2}$) + H_2 (R_{-1}). Comparison with available literature data.

311G(d,p) levels of theory are 7.3×10^{-12}, 1.4×10^{-11}, 1.1×10^{-11}, and 2.2×10^{-11} cm^3 molecule^{-1} s^{-1}, respectively. They are in very good agreement with the experimental values, which range from 1.8×10^{-11} to 2.8×10^{-11} cm^3 molecule^{-1} s^{-1}. The temperature dependence of the computed rate constants over the studied temperature range (250−1000 K) exhibits an Arrhenius behavior at almost all levels of theory, as expected in light of the experimental data. This is not particularly the case when the rate constants are calculated at the CCSD(T)/aug-cc-pVnZ//MP2/cc-pVTZ (n = T, Q, and 5) and CCSD(T)/aug-cc-pVnZ//MP2/cc-pVQZ (n = Q, and 5) levels of theory. Figure 6 presents the results of the rate constant calculations at the CCSD(T)/cc-pVnZ//MP2/cc-pVTZ (n = T and Q), CCSD(T)/6-311+G(3df,2p)//MP2/6-311G(d,p), and CCSD(T)/6-311++G(3df,3pd)//MP2/6-311G(d,p) levels of theory together with the available literature data for comparison purposes. The results shown in Figure 6 and Table 7 indicate that our calculated values at the CCSD(T)/cc-pVQZ//MP2/cc-pVTZ, CCSD(T)/6-311+G-(3df,2p)//MP2/6-311G(d,p), and 6-311++G(3df,3pd)//MP2/6-311G(d,p) are in good agreement with the measured rate constants.[17−19] Baulch et al.[16] extrapolated at high temperatures (600−1000 K) the rate constants measured by Lorenz et al.[19] at lower temperatures (250−373 K). As shown in Figure 6, a marked curvature is observed above 500 K at all levels of theory.

HI + OH → I ($^2P_{3/2}$) + H_2O (R_{-2}). Table 8 lists the rate constants calculated at 21 levels of theory for 3 different temperatures (250, 300, and 350 K) and the literature values taken from the measurements of Campuzano-Jost and Crowley[20] and the review of Atkinson et al.[25] As shown in Table 8, the difference at all temperatures between the computed rate constants and their literature counterparts are far less than an order of magnitude for almost all levels of theory, with the exception of the CCSD(T)/6-311G(d,p) single-point energy calculations. In particular, the values of the rate constants calculated at 300 K at the CCSD(T)/cc-pVnZ//MP2/cc-pVTZ (n = T and Q), CCSD(T)/6-311+G(3df,2p)//MP2/6-311G(d,p), and CCSD(T)/6-311++G(3df,3pd)//MP2/6-311G(d,p) levels of theory are 1.9×10^{-11}, 4.2×10^{-11}, 7.6×10^{-11}, and 1.3×10^{-10} cm^3 molecule^{-1} s^{-1}, respectively. They are in very good agreement with the literature values given in Table 1, which range from 9×10^{-12} to 6.9×10^{-11} cm^3 molecule^{-1} s^{-1}. Figure 7 presents the results of the rate constant calculations at the CCSD(T)/cc-pVnZ//MP2/cc-pVTZ (n = T and Q), CCSD(T)/6-311+G(3df,2p)//MP2/6-311G(d,p), and CCSD(T)/6-311++G(3df,3pd)//MP2/6-311G(d,p) levels of theory together with the available literature data for comparison purposes. The temperature dependence of the computed rate constants over the studied temperature range (250−400 K) exhibits a non-Arrhenius behavior at all levels of theory, as expected in light of the

TABLE 8: Calculated Rate Constants at Different Temperatures in cm^3 molecule^{-1} s^{-1} at Different Levels of Theory for the Reaction HI + OH → I ($^2P_{3/2}$) + H_2O (R_{-2}) and a Comparison with Literature Data

	temperature (K)		
SPC level of theory	250	300	350
CCSD(T)/cc-pVTZ//MP2/cc-pVTZ	2.0×10^{-11}	1.9×10^{-11}	1.9×10^{-11}
CCSD(T)/cc-pVQZ//MP2/cc-pVTZ	5.2×10^{-11}	4.2×10^{-11}	3.7×10^{-11}
CCSD(T)/aug-cc-pVTZ//MP2/cc-pVTZ	2.8×10^{-10}	1.7×10^{-10}	1.3×10^{-10}
CCSD(T)/cc-pVQZ//MP2/cc-pVQZ	4.9×10^{-11}	4.2×10^{-11}	3.8×10^{-11}
CCSD(T)/6-311G(d,p)//MP2/6-311G(d,p)	1.2×10^{-12}	1.7×10^{-12}	2.2×10^{-12}
CCSD(T)/6-311+G(3df,2p)//MP2/6-311G(d,p)	1.1×10^{-10}	7.6×10^{-11}	5.9×10^{-11}
CCSD(T)/6-311++G(3df,3pd)//MP2/6-311G(d,p)	2.2×10^{-10}	1.3×10^{-10}	9.4×10^{-11}
CCSD(T)/cc-pVTZ//MPW1K/cc-pVTZ	6.6×10^{-12}	8.3×10^{-12}	1.0×10^{-11}
CCSD(T)/cc-pVQZ//MPW1K/cc-pVTZ	1.3×10^{-11}	1.4×10^{-11}	1.6×10^{-11}
CCSD(T)/aug-cc-pVTZ//MPW1K/cc-pVTZ	5.2×10^{-11}	4.6×10^{-11}	4.4×10^{-11}
CCSD(T)/cc-pVQZ//MPW1K/cc-pVQZ	1.8×10^{-11}	2.0×10^{-11}	2.2×10^{-11}
CCSD(T)/6-311G(d,p)//MPW1K/6-311G(d,p)	3.7×10^{-13}	7.0×10^{-13}	1.1×10^{-12}
CCSD(T)/6-311+G(3df,2p)//MPW1K/6-311G(d,p)	6.1×10^{-12}	7.2×10^{-12}	8.4×10^{-12}
CCSD(T)/6-311++G(3df,3pd)//MPW1K/6-311G(d,p)	7.8×10^{-12}	8.8×10^{-12}	1.0×10^{-11}
CCSD(T)/cc-pVTZ//BHandHLYP/cc-pVTZ	1.3×10^{-11}	1.5×10^{-11}	1.6×10^{-11}
CCSD(T)/cc-pVQZ//BHandHLYP/cc-pVTZ	3.1×10^{-11}	2.9×10^{-11}	2.8×10^{-11}
CCSD(T)/aug-cc-pVTZ//BHandHLYP/cc-pVTZ	1.6×10^{-10}	1.1×10^{-10}	9.3×10^{-11}
CCSD(T)/cc-pVQZ//BHandHLYP/cc-pVQZ	4.9×10^{-11}	4.5×10^{-11}	4.4×10^{-11}
CCSD(T)/6-311G(d,p)//BHandHLYP/6-311G(d,p)	4.8×10^{-13}	8.3×10^{-13}	1.3×10^{-12}
CCSD(T)/6-311+G(3df,2p)//BHandHLYP/6-311G(d,p)	2.6×10^{-11}	2.3×10^{-11}	2.2×10^{-11}
CCSD(T)/6-311++G(3df,3pd)//BHandHLYP/6-311G(d,p)	4.3×10^{-11}	3.5×10^{-11}	3.2×10^{-11}
Campuzano-Jost and Crowley, 1999 [ref 20, *experiment*]	*9.1×10^{-11}*	*6.9×10^{-11}*	*5.5×10^{-11}*
Atkinson et al., 2007 [ref 25, *evaluation*]	*9.3×10^{-11}*	*6.9×10^{-11}*	*5.6×10^{-11}*

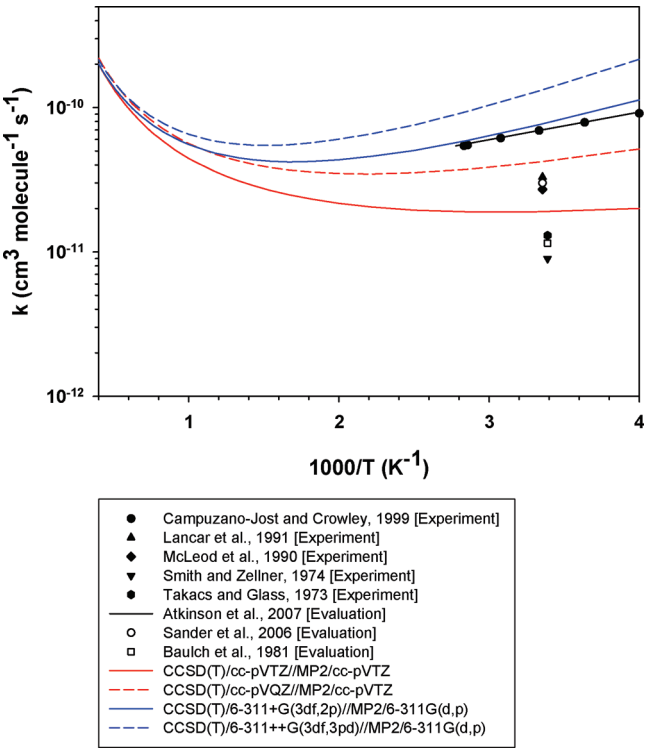

Figure 7. Temperature dependence of the rate constant of the reaction HI + OH → I ($^2P_{3/2}$) + H_2O (R_{-2}). Comparison with available literature data.

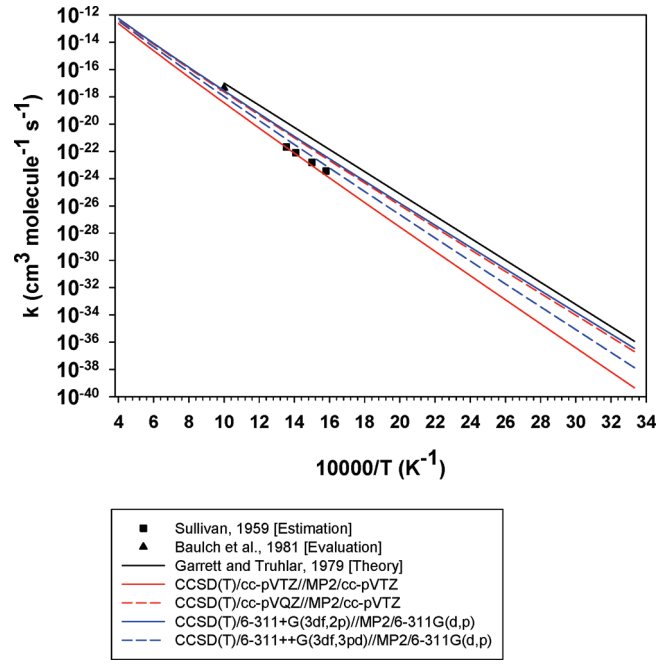

Figure 8. Temperature dependence of the rate constant of the reaction I ($^2P_{3/2}$) + HI → H + I_2 (R_3). Comparison with available literature data.

experimental data obtained by Campuzano-Jost and Crowley.[20] The rate constants calculated at the CCSD(T)/6-311+G(3df,2p)//MP2/6-311G(d,p) level of theory are especially in excellent agreement with these measured values.

I ($^2P_{3/2}$) + HI → H + I_2 (R_3). Table 9 lists the rate constants calculated at 13 levels of theory for 4 different temperatures (300, 500, 700, and 1000 K). The rate constant of this reaction has not been previously determined from experiments. Only two estimations[15,16] and a theoretical study[27] based on the BEBO method (Bond Energy−Bond Order) have been reported in the literature and are listed in Table 9 for comparison purposes. First, it can be observed that at 700 K, the literature values are different by nearly 2 orders of magnitude. A closer agreement is observed at 1000 K between the literature values (4.4×10^{-18} and 1.0×10^{-17} cm^3 molecule^{-1} s^{-1}). As shown in Table 9, the computed rate constants at 1000 K range from 10^{-20} to 10^{-18} cm^3 molecule^{-1} s^{-1}. In particular, the values of the rate constants at 1000 K calculated at the CCSD(T)/cc-pVnZ//MP2/cc-pVTZ (n = T and Q), CCSD(T)/6-311+G(3df,2p)//MP2/6-311G(d,p), and CCSD(T)/6-311++G(3df,3pd)//MP2/6-311G(d,p) levels of theory are 3.7×10^{-19}, 2.3×10^{-18}, 2.8×10^{-18}, and 1.1×10^{-18} cm^3 molecule^{-1} s^{-1}, respectively. They are in very good agreement with the value estimated by Baulch and co-workers.[16] Figure 8 presents the results of the rate constant calculations at the CCSD(T)/cc-pVnZ//MP2/cc-pVTZ (n = T and Q), CCSD(T)/6-311+G(3df,2p)//MP2/6-311G(d,p), and CCSD(T)/6-311++G(3df,3pd)//MP2/6-311G(d,p) levels of theory. The literature data taken from Sullivan,[15] Baulch et al.,[16] and Garrett and Truhlar[27] are also shown for comparison purposes. The results shown in Figure 8 and Table 9 indicate that our calculated values are in very good agreement with the literature data. The rate constants

TABLE 9: Calculated Rate Constants at Different Temperatures in cm^3 molecule^{-1} s^{-1} at Different Levels of Theory for the Reaction I ($^2P_{3/2}$) + HI → H + I_2 (R_3) and a Comparison with Literature Data

	temperature (K)			
SPC level of theory	300	500	700	1000
CCSD(T)/cc-pVTZ//MP2/cc-pVTZ	4.5×10^{-40}	2.8×10^{-28}	4.1×10^{-23}	3.7×10^{-19}
CCSD(T)/cc-pVQZ//MP2/cc-pVTZ	2.0×10^{-37}	1.1×10^{-26}	5.6×10^{-22}	2.3×10^{-18}
CCSD(T)/cc-pV5Z//MP2/cc-pVTZ	2.5×10^{-36}	5.0×10^{-26}	1.7×10^{-21}	4.9×10^{-18}
CCSD(T)/aug-cc-pVTZ//MP2/cc-pVTZ	1.1×10^{-38}	1.9×10^{-27}	1.6×10^{-22}	9.7×10^{-19}
CCSD(T)/aug-cc-pVQZ//MP2/cc-pVTZ	1.6×10^{-36}	3.8×10^{-26}	1.4×10^{-21}	4.3×10^{-18}
CCSD(T)/aug-cc-pV5Z//MP2/cc-pVTZ	4.1×10^{-36}	6.7×10^{-26}	2.1×10^{-21}	5.8×10^{-18}
CCSD(T)/cc-pVQZ//MP2/cc-pVQZ	1.2×10^{-37}	7.6×10^{-27}	4.2×10^{-22}	1.9×10^{-18}
CCSD(T)/cc-pV5Z//MP2/cc-pVQZ	1.5×10^{-36}	3.6×10^{-26}	1.3×10^{-21}	4.0×10^{-18}
CCSD(T)/aug-cc-pVQZ//MP2/cc-pVQZ	8.6×10^{-37}	2.5×10^{-26}	1.0×10^{-21}	3.4×10^{-18}
CCSD(T)/aug-cc-pV5Z//MP2/cc-pVQZ	2.4×10^{-36}	4.8×10^{-26}	1.6×10^{-21}	4.6×10^{-18}
CCSD(T)/6-311G(d,p)//MP2/6-311G(d,p)	1.2×10^{-43}	2.0×10^{-30}	1.2×10^{-24}	3.2×10^{-20}
CCSD(T)/6-311+G(3df,2p)//MP2/6-311G(d,p)	3.5×10^{-37}	1.6×10^{-26}	7.3×10^{-22}	2.8×10^{-18}
CCSD(T)/6-311++G(3df,3pd)//MP2/6-311G(d,p)	1.4×10^{-38}	2.2×10^{-27}	1.8×10^{-22}	1.1×10^{-18}
Garrett and Truhlar, 1979 [ref 27, *theory*]	*1.2×10^{-36}*	*7.7×10^{-26}*	*3.4×10^{-21}*	*1.0×10^{-17}*
Sullivan, 1959 [ref 15, *estimation*]			*5.5×10^{-23}*	
Baulch et al., 1981 [ref 16, *evaluation*]				*4.4×10^{-18}*

TABLE 10: Calculated Rate Constants at Different Temperatures in cm^3 molecule^{-1} s^{-1} at Different Levels of Theory for the Reaction H + I_2 → I ($^2P_{3/2}$) + HI (R_{-3}) and a Comparison with Literature Data

	temperature (K)			
SPC level of theory	300	400	600	800
CCSD(T)/cc-pVTZ//MP2/cc-pVTZ	6.6×10^{-11}	8.7×10^{-11}	1.3×10^{-10}	1.8×10^{-10}
CCSD(T)/cc-pVQZ//MP2/cc-pVTZ	3.4×10^{-10}	3.0×10^{-10}	3.0×10^{-10}	3.3×10^{-10}
CCSD(T)/cc-pV5Z//MP2/cc-pVTZ	6.4×10^{-10}	4.8×10^{-10}	4.1×10^{-10}	4.2×10^{-10}
CCSD(T)/aug-cc-pVTZ//MP2/cc-pVTZ	7.3×10^{-10}	5.3×10^{-10}	4.4×10^{-10}	4.5×10^{-10}
CCSD(T)/aug-cc-pVQZ//MP2/cc-pVTZ	1.7×10^{-9}	1.0×10^{-9}	6.8×10^{-10}	6.2×10^{-10}
CCSD(T)/aug-cc-pV5Z//MP2/cc-pVTZ	2.7×10^{-9}	1.4×10^{-9}	8.5×10^{-10}	7.3×10^{-10}
CCSD(T)/cc-pVQZ//MP2/cc-pVQZ	2.0×10^{-10}	2.0×10^{-10}	2.2×10^{-10}	2.7×10^{-10}
CCSD(T)/cc-pV5Z//MP2/cc-pVQZ	3.8×10^{-10}	3.2×10^{-10}	2.3×10^{-10}	3.4×10^{-10}
CCSD(T)/aug-cc-pVQZ//MP2/cc-pVQZ	9.9×10^{-10}	6.6×10^{-10}	2.4×10^{-10}	4.8×10^{-10}
CCSD(T)/aug-cc-pV5Z//MP2/cc-pVQZ	1.5×10^{-9}	9.2×10^{-10}	2.5×10^{-10}	5.7×10^{-10}
CCSD(T)/6-311G(d,p)//MP2/6-311G(d,p)	4.8×10^{-12}	1.2×10^{-11}	3.5×10^{-11}	6.6×10^{-11}
CCSD(T)/6-311+G(3df,2p)//MP2/6-311G(d,p)	1.2×10^{-10}	1.3×10^{-10}	1.7×10^{-10}	2.2×10^{-10}
CCSD(T)/6-311++G(3df,3pd)//MP2/6-311G(d,p)	3.8×10^{-10}	3.2×10^{-10}	3.1×10^{-10}	3.4×10^{-10}
Lorenz et al., 1979 [ref 19, *experiment*]	*6.2×10^{-10}*	*6.3×10^{-10}*		
Baulch et al., 1981 [ref 16, *evaluation*]			*5.0×10^{-10}*	*5.5×10^{-10}*

obtained from previous theoretical work of Garrett and Truhlar[27] are higher than the ones computed in this work over the temperature range of 500−1000 K. At 300 K, the opposite trend is observed with the values calculated at the CCSD(T)/aug-cc-pVnZ//MP2/cc-pVTZ (n = Q and 5) and CCSD(T)/aug-cc-pV5Z//MP2/cc-pVQZ levels of theory. The values computed at the CCSD(T)/6-311+G(3df,2p)//MP2/6-311G(d,p) level of theory are about one-third smaller than the ones predicted by Garrett and Truhlar[27] over the whole temperature range.

H + I_2 → I ($^2P_{3/2}$) + HI (R_{-3}). Table 10 lists the rate constants calculated at 13 levels of theory for 4 different temperatures (300, 400, 600, and 800 K), together with the available literature data.[16,19] As shown in Table 10, the computed rate constants range from 10^{-12} to 10^{-9} cm^3 molecule^{-1} s^{-1} at 300 K. The values of the rate constants calculated at the CCSD(T)/cc-pVnZ//MP2/cc-pVTZ (n = T and Q), CCSD(T)/6-311+G(3df,2p)//MP2/6-311G(d,p), and CCSD(T)/6-311++G(3df,3pd)//MP2/6-311G(d,p) levels of theory are 6.6×10^{-11}, 3.4×10^{-10}, 1.2×10^{-10}, and 3.8×10^{-10} cm^3 molecule^{-1} s^{-1}, respectively, at 300 K. They are very close to the measured value by Lorenz and co-workers[19] (6.2×10^{-10} cm^3 molecule^{-1} s^{-1}). The temperature dependence of the computed rate constants over the temperature range of 300−400 K exhibit a non-Arrhenius behavior at almost all levels of theory. The few experimental data from Lorenz et al.[19] show that the rate constants do not depend on the temperature in this range. Figure 9 presents the results of the rate constant calculations at the CCSD(T)/cc-pVnZ//MP2/cc-pVTZ (n = T and Q), CCSD(T)/6-311+G(3df,2p)//MP2/6-311G(d,p), and CCSD(T)/6-311++G(3df,3pd)//MP2/6-311G(d,p) levels of theory together with the available literature data for comparison purposes. The results shown in Figure 9 and Table 10 indicate that the difference between our calculated values at the CCSD(T)/cc-pVTZ//MP2/cc-pVTZ and CCSD(T)/6-311+G(3df,2p)//MP2/6-311G(d,p) levels of theory and their literature counterparts is about 1 order of magnitude. A better agreement is observed for the rate constants calculated at the CCSD(T)/cc-pVQZ/MP2/cc-pVTZ and CCSD(T)/6-311++G(3df,3pd)//MP2/6-311G(d,p) levels of theory, although the computed rate constants exhibit a non-Arrhenius behavior over the temperature range of 250−400 K.

HI + O (^3P) → I ($^2P_{3/2}$) + OH (R_{-4}). Table 11 lists the rate constants calculated at 39 levels of theory for 4 different temperatures (300, 400, 500, and 550 K), together with the available literature values.[28,29] As shown in Table 11, the computed rate constants range from 10^{-16} to 10^{-11} cm^3 molecule^{-1} s^{-1} at 300 K. The differences at all temperatures

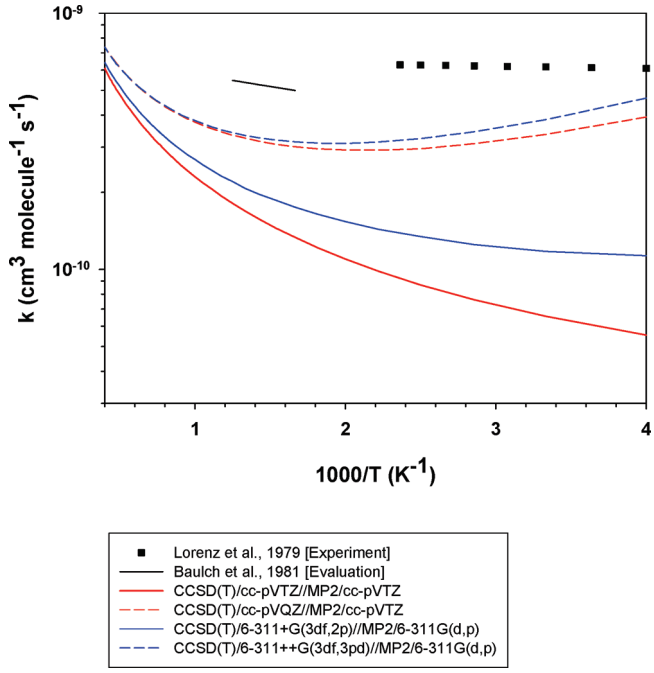

Figure 9. Temperature dependence of the rate constant of the reaction H + I_2 → I ($^2P_{3/2}$) + HI (R_{-3}). Comparison with available literature data.

between the computed rate constants and their literature counterparts are far less than an order of magnitude for almost all levels of theory, with the exception of the CCSD(T)/6-311G(d,p) single-point energy calculations. The values of the rate constants calculated at the CCSD(T)/cc-pVnZ//MP2/cc-pVTZ (n = T and Q), CCSD(T)/6-311+G(3df,2p)//MP2/6-311G(d,p), and CCSD(T)/6-311++G(3df,3pd)//MP2/6-311G(d,p) levels of theory are 1.8×10^{-13}, 7.3×10^{-11}, 1.1×10^{-12}, and 3.0×10^{-12} cm^3 molecule^{-1} s^{-1}, respectively, at 300 K. They are in good agreement with the experimental value determined by Singleton and Cvetanovic (1.7×10^{-12} cm^3 molecule^{-1} s^{-1}).[28] The temperature dependence of the computed rate constants over the studied temperature range (300−550 K) exhibits an Arrhenius behavior at all levels of theory, as expected in light of the literature data. Figure 10 presents the results of the rate constant calculations at the CCSD(T)/cc-pVnZ//MP2/cc-pVTZ (n = T and Q), CCSD(T)/6-311+G(3df,2p)//MP2/6-311G(d,p), and CCSD(T)/6-311++G(3df,3pd)//MP2/6-311G(d,p) levels of theory together with the available literature data for comparison

TABLE 11: Calculated Rate Constants at Different Temperatures in cm^3 molecule^{-1} s^{-1} at Different Levels of Theory for the Reaction HI + O (^{3}P) → I ($^2P_{3/2}$) + OH (R_{-4}) and a Comparison with Literature Data

SPC level of theory	temperature (K)			
	300	400	500	550
CCSD(T)/cc-pVTZ//MP2/cc-pVTZ	1.8×10^{-13}	6.4×10^{-13}	1.5×10^{-12}	2.0×10^{-12}
CCSD(T)/cc-pVQZ//MP2/cc-pVTZ	7.3×10^{-13}	1.9×10^{-12}	3.4×10^{-12}	4.4×10^{-12}
CCSD(T)/cc-pV5Z//MP2/cc-pVTZ	1.1×10^{-12}	2.5×10^{-12}	4.3×10^{-12}	5.4×10^{-12}
CCSD(T)/aug-cc-pVTZ//MP2/cc-pVTZ	4.9×10^{-12}	7.7×10^{-12}	1.1×10^{-11}	1.2×10^{-11}
CCSD(T)/aug-cc-pVQZ//MP2/cc-pVTZ	1.2×10^{-11}	1.5×10^{-11}	1.9×10^{-11}	2.0×10^{-11}
CCSD(T)/aug-cc-pV5Z//MP2/cc-pVTZ	1.1×10^{-11}	1.4×10^{-11}	1.7×10^{-11}	1.9×10^{-11}
CCSD(T)/cc-pVQZ//MP2/cc-pVQZ	6.2×10^{-13}	1.7×10^{-12}	3.2×10^{-12}	4.1×10^{-12}
CCSD(T)/cc-pV5Z//MP2/cc-pVQZ	8.8×10^{-13}	2.2×10^{-12}	3.9×10^{-12}	4.9×10^{-12}
CCSD(T)/aug-cc-pVQZ//MP2/cc-pVQZ	1.0×10^{-11}	1.3×10^{-11}	1.7×10^{-11}	1.9×10^{-11}
CCSD(T)/aug-cc-pV5Z//MP2/cc-pVQZ	8.2×10^{-12}	1.1×10^{-11}	1.5×10^{-11}	1.7×10^{-11}
CCSD(T)/6-311G(d,p)//MP2/6-311G(d,p)	1.9×10^{-15}	2.1×10^{-14}	9.6×10^{-14}	1.7×10^{-13}
CCSD(T)/6-311+G(3df,2p)//MP2/6-311G(d,p)	1.1×10^{-12}	2.6×10^{-12}	4.5×10^{-12}	5.6×10^{-12}
CCSD(T)/6-311++G(3df,3pd)//MP2/6-311G(d,p)	3.0×10^{-12}	5.5×10^{-12}	8.1×10^{-12}	9.6×10^{-12}
CCSD(T)/cc-pVTZ//MPW1K/cc-pVTZ	2.7×10^{-14}	1.7×10^{-13}	5.6×10^{-13}	8.7×10^{-13}
CCSD(T)/cc-pVQZ//MPW1K/cc-pVTZ	8.9×10^{-14}	4.2×10^{-13}	1.1×10^{-12}	1.7×10^{-12}
CCSD(T)/cc-pV5Z//MPW1K/cc-pVTZ	1.2×10^{-13}	5.2×10^{-13}	1.4×10^{-12}	2.0×10^{-12}
CCSD(T)/aug-cc-pVTZ//MPW1K/cc-pVTZ	4.5×10^{-13}	1.4×10^{-12}	3.0×10^{-12}	4.1×10^{-12}
CCSD(T)/aug-cc-pVQZ//MPW1K/cc-pVTZ	9.0×10^{-13}	2.4×10^{-12}	4.6×10^{-12}	5.9×10^{-12}
CCSD(T)/aug-cc-pV5Z//MPW1K/cc-pVTZ	7.6×10^{-13}	2.1×10^{-12}	4.1×10^{-12}	5.4×10^{-12}
CCSD(T)/cc-pVQZ//MPW1K/cc-pVQZ	9.6×10^{-14}	4.5×10^{-13}	1.2×10^{-12}	1.8×10^{-12}
CCSD(T)/cc-pV5Z//MPW1K/cc-pVQZ	1.3×10^{-13}	5.5×10^{-13}	1.4×10^{-12}	2.0×10^{-12}
CCSD(T)/aug-cc-pVQZ//MPW1K/cc-pVQZ	9.8×10^{-13}	2.6×10^{-12}	4.9×10^{-12}	6.3×10^{-12}
CCSD(T)/aug-cc-pV5Z//MPW1K/cc-pVQZ	8.3×10^{-13}	2.3×10^{-12}	4.4×10^{-12}	5.7×10^{-12}
CCSD(T)/6-311G(d,p)//MPW1K/6-311G(d,p)	3.7×10^{-16}	6.7×10^{-15}	4.0×10^{-14}	7.9×10^{-14}
CCSD(T)/6-311+G(3df,2p)//MPW1K/6-311G(d,p)	6.5×10^{-14}	3.2×10^{-13}	8.9×10^{-13}	1.3×10^{-12}
CCSD(T)/6-311++G(3df,3pd)//MPW1K/6-311G(d,p)	1.4×10^{-13}	5.7×10^{-13}	1.4×10^{-12}	2.0×10^{-12}
CCSD(T)/cc-pVTZ//BHandHLYP/cc-pVTZ	5.1×10^{-14}	2.6×10^{-13}	7.6×10^{-13}	1.1×10^{-12}
CCSD(T)/cc-pVQZ//BHandHLYP/cc-pVTZ	1.7×10^{-13}	6.5×10^{-13}	1.6×10^{-12}	2.2×10^{-12}
CCSD(T)/cc-pV5Z//BHandHLYP/cc-pVTZ	2.2×10^{-13}	7.9×10^{-13}	1.8×10^{-12}	2.5×10^{-12}
CCSD(T)/aug-cc-pVTZ//BHandHLYP/cc-pVTZ	1.0×10^{-12}	2.5×10^{-12}	4.6×10^{-12}	5.9×10^{-12}
CCSD(T)/aug-cc-pVQZ//BHandHLYP/cc-pVTZ	2.3×10^{-12}	4.6×10^{-12}	7.5×10^{-12}	9.0×10^{-12}
CCSD(T)/aug-cc-pV5Z//BHandHLYP/cc-pVTZ	2.0×10^{-12}	4.2×10^{-12}	6.9×10^{-12}	8.5×10^{-12}
CCSD(T)/cc-pVQZ//BHandHLYP/cc-pVQZ	1.7×10^{-13}	6.6×10^{-13}	1.6×10^{-12}	2.2×10^{-12}
CCSD(T)/cc-pV5Z//BHandHLYP/cc-pVQZ	2.2×10^{-13}	8.0×10^{-13}	1.8×10^{-12}	2.6×10^{-12}
CCSD(T)/aug-cc-pVQZ//BHandHLYP/cc-pVQZ	2.5×10^{-12}	4.9×10^{-12}	7.9×10^{-12}	9.6×10^{-12}
CCSD(T)/aug-cc-pV5Z//BHandHLYP/cc-pVQZ	2.3×10^{-12}	4.6×10^{-12}	7.5×10^{-12}	9.2×10^{-12}
CCSD(T)/6-311G(d,p)//BHandHLYP/6-311G(d,p)	7.2×10^{-16}	1.1×10^{-14}	5.8×10^{-14}	1.1×10^{-13}
CCSD(T)/6-311+G(3df,2p)//BHandHLYP/6-311G(d,p)	1.9×10^{-13}	7.1×10^{-13}	1.7×10^{-12}	2.3×10^{-12}
CCSD(T)/6-311++G(3df,3pd)//BHandHLYP/6-311G(d,p)	4.7×10^{-13}	1.4×10^{-12}	2.8×10^{-12}	3.7×10^{-12}
Singleton and Cvetanovic, 1978 [ref 28, *experiment*]	1.7×10^{-12}	3.8×10^{-12}	6.3×10^{-12}	7.6×10^{-12}
Persky and Broida, 1987 [ref 29, *theory*]	1.6×10^{-12}	3.0×10^{-12}	4.2×10^{-12}	

purposes. The results shown in Figure 10 and Table 11 indicate that the rate constants computed with the CCSD(T)/cc-pVQZ, CCSD(T)/6-311+G(3df,2p), and CCSD(T)/6-311++G(3df,3pd) single-point energy calculations are in better agreement with the rate constants from the literature.[28,29] The rate constants calculated at the CCSD(T)/cc-pVTZ//MP2/cc-pVTZ level are slightly lower than the other ones and their literature counterparts.

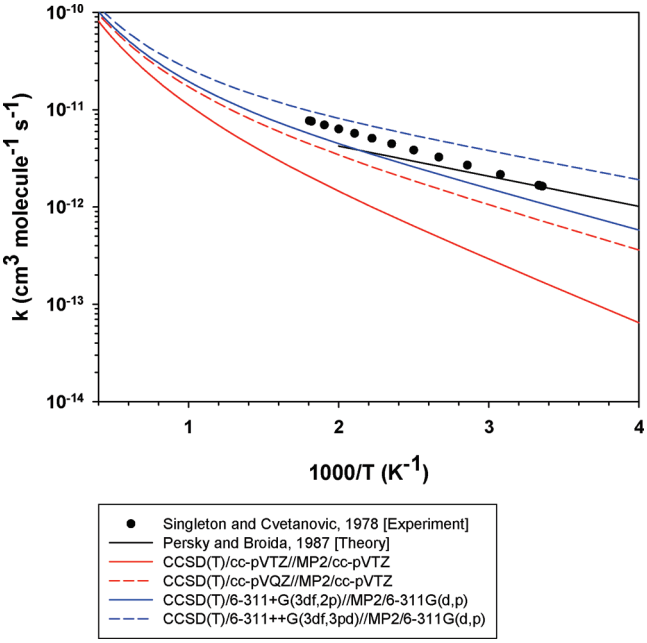

Figure 10. Temperature dependence of the rate constant of the reaction HI + O (^{3}P) → I ($^2P_{3/2}$) + OH (R_{-4}). Comparison with available literature data.

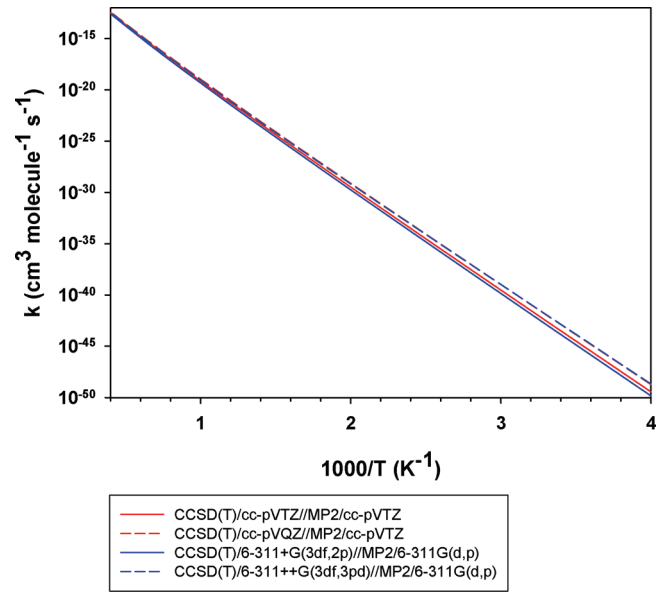

Figure 11. Temperature dependence of the rate constant of the reaction I ($^2P_{3/2}$) + H_2O → HI + OH (R_2).

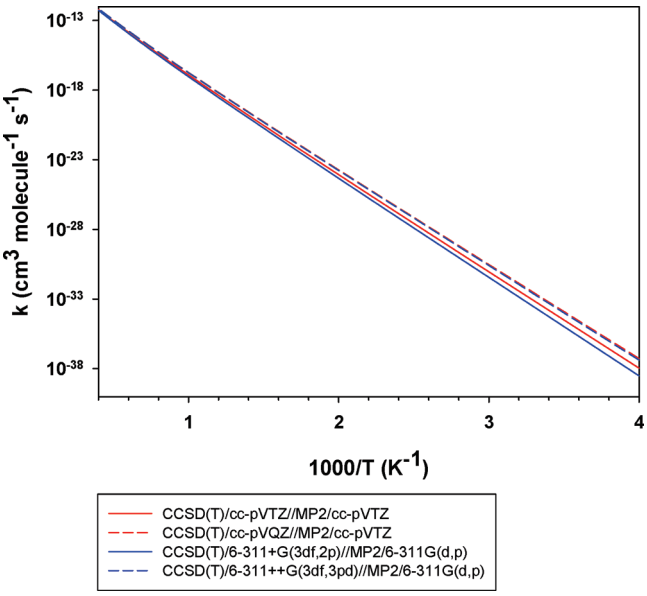

Figure 12. Temperature dependence of the rate constant of the reaction I ($^2P_{3/2}$) + OH → HI + O (^3P) (R_4).

I ($^2P_{3/2}$) + H_2O → HI + OH (R_2) and I ($^2P_{3/2}$) + OH → HI + O (^3P) (R_4). Figures 11 and 12 present the results of the rate constant calculations at the CCSD(T)/cc-pVnZ//MP2/cc-pVTZ (n = T and Q), CCSD(T)/6-311+G(3df,2p)//MP2/6-311G(d,p), and CCSD(T)/6-311++G(3df,3pd)//MP2/6-311G(d,p) levels of theory. To the best of our knowledge, no experimental data are available for these reactions. The calculated rate constants with the four levels of theory are consistent.

Arrhenius Parameters. The modified three-parameter Arrhenius expressions $k(T) = A \times T^n \exp(-E_a/RT)$ fitted to the rate constants computed at the four levels of theory over the temperature range of 250−2500 K are reported in Table 12. On the basis of the very good agreement observed between our calculated rate constants and the available literature values (see discussion above), we are confident in our predicted Arrhenius parameters with the four different levels of theory for the eight elementary reactions under study.

Conclusion

Ab initio and DFT theoretical calculations combined with canonical TST were performed on the reactions of I atoms with H_2, H_2O, HI, and OH. The geometry parameters for reactants, products, molecular complexes, and TSs were fully optimized with the MP2, MPW1K, and BHandHLYP methods combined with different basis sets. In this paper, we showed that standard theoretical methods were adequate to obtain quantitative rate constants for the reaction under study. In particular, the calculated rate constants using the CCSD(T)/cc-pVnZ//MP2/cc-pVTZ (n = T and Q), CCSD(T)/6-311+G(3df,2p)//MP2/6-311G(d,p), and CCSD(T)/6-311++G(3df,3pd)//MP2/6-311G(d,p) levels of theory are close to their literature counterparts. The use of the CCSD(T)/cc-pVQZ//MP2/cc-pVTZ and CCSD(T)/6-311++G(3df,3pd) levels of theory allows one to obtain a better agreement with the literature data for all reactions, with the exception of the I + H_2 reaction R_1. The rate constants

TABLE 12: Summary of the Arrhenius Parameters Calculated over the Temperature Range of 250−2500 K for the Studied Reactions

reaction	SPC level of theory	A^a	n	$E_a{}^b$
I ($^2P_{3/2}$) + H_2 → HI + H (R_1)	CCSD(T)/cc-pVTZ//MP2/cc-pVTZ	4.0×10^{-16}	1.93	137.3
	CCSD(T)/cc-pVQZ//MP2/cc-pVTZ	4.0×10^{-16}	1.93	128.2
	CCSD(T)/6-311+G(3df,2p)//MP2/6-311G(d,p)	2.2×10^{-16}	2.00	134.9
	CCSD(T)/6-311++G(3df,3pd)//MP2/6-311G(d,p)	2.2×10^{-16}	2.00	128.3
HI + H → I ($^2P_{3/2}$) + H_2 (R_{-1})	CCSD(T)/cc-pVTZ//MP2/cc-pVTZ	3.6×10^{-16}	1.68	−0.8
	CCSD(T)/cc-pVQZ//MP2/cc-pVTZ	3.6×10^{-16}	1.68	−2.3
	CCSD(T)/6-311+G(3df,2p)//MP2/6-311G(d,p)	2.0×10^{-16}	1.75	−2.4
	CCSD(T)/6-311++G(3df,3pd)//MP2/6-311G(d,p)	2.0×10^{-16}	1.75	−4.0
I ($^2P_{3/2}$) + H_2O → HI + OH (R_2)	CCSD(T)/cc-pVTZ//MP2/cc-pVTZ	5.1×10^{-17}	2.26	184.7
	CCSD(T)/cc-pVQZ//MP2/cc-pVTZ	5.2×10^{-17}	2.26	181.2
	CCSD(T)/6-311+G(3df,2p)//MP2/6-311G(d,p)	1.4×10^{-17}	2.40	185.4
	CCSD(T)/6-311++G(3df,3pd)//MP2/6-311G(d,p)	1.4×10^{-17}	2.40	179.8
HI + OH → I ($^2P_{3/2}$) + H_2O (R_{-2})	CCSD(T)/cc-pVTZ//MP2/cc-pVTZ	1.2×10^{-17}	2.09	−5.9
	CCSD(T)/cc-pVQZ//MP2/cc-pVTZ	1.2×10^{-17}	2.09	−7.9
	CCSD(T)/6-311+G(3df,2p)//MP2/6-311G(d,p)	3.3×10^{-18}	2.23	−10.6
	CCSD(T)/6-311++G(3df,3pd)//MP2/6-311G(d,p)	3.3×10^{-18}	2.22	−11.9
I ($^2P_{3/2}$) + HI → H + I_2 (R_3)	CCSD(T)/cc-pVTZ//MP2/cc-pVTZ	9.6×10^{-16}	1.72	164.2
	CCSD(T)/cc-pVQZ//MP2/cc-pVTZ	9.7×10^{-16}	1.72	149.0
	CCSD(T)/6-311+G(3df,2p)//MP2/6-311G(d,p)	8.5×10^{-16}	1.74	147.7
	CCSD(T)/6-311++G(3df,3pd)//MP2/6-311G(d,p)	8.3×10^{-16}	1.74	155.7
H + I_2 → I ($^2P_{3/2}$) + HI (R_{-3})	CCSD(T)/cc-pVTZ//MP2/cc-pVTZ	1.3×10^{-13}	1.09	−0.2
	CCSD(T)/cc-pVQZ//MP2/cc-pVTZ	1.2×10^{-13}	1.09	−4.3
	CCSD(T)/6-311+G(3df,2p)//MP2/6-311G(d,p)	9.8×10^{-14}	1.11	−1.9
	CCSD(T)/6-311++G(3df,3pd)//MP2/6-311G(d,p)	9.9×10^{-14}	1.11	−4.8
I ($^2P_{3/2}$) + OH → HI + O (^3P) (R_4)	CCSD(T)/cc-pVTZ//MP2/cc-pVTZ	4.7×10^{-16}	1.70	127.7
	CCSD(T)/cc-pVQZ//MP2/cc-pVTZ	4.7×10^{-16}	1.70	124.4
	CCSD(T)/6-311+G(3df,2p)//MP2/6-311G(d,p)	5.1×10^{-16}	1.69	130.4
	CCSD(T)/6-311++G(3df,3pd)//MP2/6-311G(d,p)	5.2×10^{-16}	1.69	125.0
HI + O (^3P) → I ($^2P_{3/2}$) + OH (R_{-4})	CCSD(T)/cc-pVTZ//MP2/cc-pVTZ	9.8×10^{-16}	1.50	8.4
	CCSD(T)/cc-pVQZ//MP2/cc-pVTZ	9.6×10^{-16}	1.50	4.9
	CCSD(T)/6-311+G(3df,2p)//MP2/6-311G(d,p)	1.1×10^{-15}	1.49	3.9
	CCSD(T)/6-311++G(3df,3pd)//MP2/6-311G(d,p)	1.1×10^{-15}	1.49	1.5

[a] Units: cm^3 $molecule^{-1}$ s^{-1}. [b] Units: kJ mol^{-1}.

computed over the temperature range of 250−2500 K have been fitted with a modified three-parameter Arrhenius expression. These Arrhenius parameters are therefore recommended for use in the development of a gaseous kinetic network, which could be implemented in severe accident simulation software such as ASTEC[7]/SOPHAEROS,[8] for instance.

Acknowledgment. We thank the Grand Equipement National de Calcul Intensif (GENCI), Institut du Développement et des Ressources en Informatique Scientifique (IDRIS), the ROMEO2 computational center of the University of Reims Champagne-Ardenne, the Centre de Ressources Informatiques de HAute Normandie (CRIHAN), and the Centre de Ressources Informatiques (CRI) of the University of Lille 1 for providing computing time for part of the theoretical calculations. We thank the Nord Pas de Calais Region, the European funds for Regional Economic Development, and the Air Quality Program of the Institut de Recherche en ENvironnment Industriel for their financial support. We are grateful to EDF for its financial support to the IRSN source term modeling program. The authors are also grateful to Dr. Eddy Thiriot and Professor Ivan Cernusak for fruitful discussions.

Supporting Information Available: Vibrational frequency scaling factors, optimized geometric parameters (reactants and products), vibrational frequencies (reactants, molecular complexes, TSs, and products), and literature enthalpies of formation at 0 K are given in the Supporting Information. This material is available free of charge via the Internet at http://pubs.acs.org.

References and Notes

(1) Wren, J. C.; Ball, J. M.; Glowa, G. A. *Nucl. Technol.* **2000**, *129*, 297–325.

(2) *Iodine Aspects of Severe Accident Management Workshop Proceedings*; OECD Nuclear Energy Agency, NEA/CNSI/R(99)7, Finland, May 18−20999.

(3) Cantrel, L.; March, P. *Nucl. Technol.* **2006**, *154*, 170–185.

(4) Clément, B.; Hanniet-Girault, N.; Repetto, G.; Jacquemain, D.; Jones, A. V.; Kissane, M. P.; von der Hardt, P. *Nucl. Eng. Des.* **2003**, *226*, 5–82.

(5) Girault, N.; Fiche, C.; Bujan, A.; Dienstbier, J. *Nucl. Eng. Des.* **2009**, *239*, 1162–1170.

(6) Clément, B.; Zeyen, R. *International Conference, Nuclear Energy for New Europe*; Bled (Slovenia), September 5−8, 2005.

(7) Van Dorsselaere, J. P.; Seropian, C.; Chatelard, P.; Jacq, F.; Fleurot, J.; Giordano, P.; Reinke, N.; Schwinges, B.; Allelein, H. J.; Luther, W. *Nucl. Technol.* **2009**, *165*, 293–307.

(8) Cousin, F.; Dieschbourg, K.; Jacq, F. *Nucl. Eng. Des.* **2008**, *238*, 2430–2438.

(9) Cantrel, L. *Potential gaseous reactions in the RCS, Part I: Kinetic Modeling of the {Cs−I−O−H}*, Internal Technical report; SEMIC-2007-099, **2007**.

(10) Michael, J. V.; Kumaran, S. S.; Su, M. C.; Lim, K. P. *Chem. Phys. Lett.* **2000**, *319*, 99–106.

(11) Inada, Y.; Akagane, K. *J. Nucl. Sci. Technol.* **1996**, *33*, 562–568.

(12) Truhlar, D. G.; Gray, J. C. *Chem. Phys. Lett.* **1978**, *57*, 93–99.

(13) Horie, O.; Ishii, Y.; Amano, A. *J. Phys. Chem.* **1964**, *68*, 1264–1266.

(14) Sullivan, J. H. *J. Chem. Phys.* **1962**, *36*, 1925–1932.

(15) Sullivan, J. H. *J. Chem. Phys.* **1959**, *30*, 1292–1300.

(16) Baulch, D. L.; Duxbury, J.; Grant, S. J.; Montague, D. C. Evaluated kinetic data for high-temperature reactions. Volume 4. Homogeneous gas phase reactions of halogen- and cyanide- containing species. *J. Phys. Chem. Ref. Data* **1981**, *10*, Suppl. 1.

(17) Vasileiadis, S.; Benson, S. W. *Int. J. Chem. Kinet.* **1997**, *29*, 915–925.

(18) Umemoto, H.; Nakagawa, S.; Tsunashima, S.; Sato, S. *Chem. Phys.* **1988**, *124*, 259–263.

(19) Lorenz, K.; Wagner, H. Gg.; Zellner, R. *Ber. Bunsen-Ges. Phys. Chem.* **1979**, *83*, 556–560.

(20) Campuzano-Jost, P.; Crowley, J. N. *J. Phys. Chem. A* **1999**, *103*, 2712–2719.

(21) Lancar, I. T.; Mellouki, A.; Poulet, G. *Chem. Phys. Lett.* **1991**, *177*, 554–558.

(22) Mac Leod, H.; Balestra, C.; Jourdain, J. L.; Laverdet, G.; Le Bras, G. *Int. J. Chem. Kinet.* **1990**, *22*, 1167–1176.

(23) Smith, I. W. M.; Zellner, R. *J. Chem. Soc., Faraday Trans.* **1974**, *70*, 1045–1056.

(24) Takacs, G. A.; Glass, G. P. *J. Phys. Chem.* **1973**, *77*, 1948–1951.

(25) Atkinson, R.; Baulch, D. L.; Cox, R. A.; Crowley, J. N.; Hampson, R. F.; Hynes, R. G.; Jenkin, M. E.; Rossi, M. J.; Troe, J. *Atmos. Chem. Phys.* **2007**, *7*, 981–1191.

(26) Sander, S. P.; Friedl, R. R.; Ravishankara, A. R.; Golden, D. M.; Kolb, C. E.; Kurylo, M. J.; Molina, M. J.; Moortgat, G. K.; Finlayson-Pitts, B. J.; Wine, P. H.; Huie, R. E.; Orkin, V. L. *Chemical kinetics and photochemical data for use in atmospheric studies*, Evaluation number 15; JPL-NASA 06-2, 2006; http://jpldataeval.jpl.nasa.gov

(27) Garrett, B. C.; Truhlar, D. G. *J. Am. Chem. Soc.* **1979**, *101*, 5207–5217.

(28) Singleton, D. L.; Cvetanovic, R. J. *Can. J. Chem.* **1978**, *56*, 2934–2939.

(29) Persky, A.; Broida, M. *Chem. Phys.* **1987**, *114*, 85–93.

(30) Frisch, M. J.; Trucks, G. W.; Schlegel, H. B.; Scuseria, G. E.; Robb, M. A.; Cheeseman, J. R.; Montgomery, J. A., Jr.; Vreven, T.; Kudin, K. N.; Burant, J. C.; Millam, J. M.; Iyengar, S. S.; Tomasi, J.; Barone, V.; Mennucci, B.; Cossi, M.; Scalmani, G.; Rega, N.; Petersson, G. A.; Nakatsuji, H.; Hada, M.; Ehara, M.; Toyota, K.; Fukuda, R.; Hasegawa, J.; Ishida, M.; Nakajima, T.; Honda, Y.; Kitao, O.; Nakai, H.; Klene, M.; Li, X.; Knox, J. E.; Hratchian, H. P.; Cross, J. B.; Bakken, V.; Adamo, C.; Jaramillo, J.; Gomperts, R.; Stratmann, R. E.; Yazyev, O.; Austin, A. J.; Cammi, R.; Pomelli, C.; Ochterski, J. W.; Ayala, P. Y.; Morokuma, K.; Voth, G. A.; Salvador, P.; Dannenberg, J. J.; Zakrzewski, V. G.; Dapprich, S.; Daniels, A. D.; Strain, M. C.; Farkas, O.; Malick, D. K.; Rabuck, A. D.; Raghavachari, K.; Foresman, J. B.; Ortiz, J. V.; Cui, Q.; Baboul, A. G.; Clifford, S.; Cioslowski, J.; Stefanov, B. B.; Liu, G.; Liashenko, A.; Piskorz, P.; Komaromi, I.; Martin, R. L.; Fox, D. J.; Keith, T.; Al-Laham, M. A.; Peng, C. Y.; Nanayakkara, A.; Challacombe, M.; Gill, P. M. W.; Johnson, B.; Chen, W.; Wong, M. W.; Gonzalez, C.; Pople, J. A. *Gaussian 03*, revision D.01; Gaussian, Inc.: Wallingford, CT, 2004.

(31) Møller, C.; Plesset, M. S. *Phys. Rev.* **1934**, *46*, 618–622.

(32) Lynch, B. J.; Fast, P. L.; Harris, M.; Truhlar, D. G. *J. Phys. Chem. A* **2000**, *104*, 4811–4815.

(33) The BHandHLYP functional defined in Gaussian03 is different from the original one in Becke's paper; see: Becke, A. D. *J. Chem. Phys.* **1993**, *98*, 1372–1377; see http://www.gaussian.com/g_tech/g_ur/k_dft.htm.

(34) (a) Dunning, T. H., Jr. *J. Chem. Phys.* **1989**, *90*, 1007–1023. (b) Kendall, R. A.; Dunning, T. H., Jr.; Harrison, R. J. *J. Chem. Phys.* **1992**, *96*, 6796–6806. (c) Woon, D. E.; Dunning, T. H., Jr. *J. Chem. Phys.* **1993**, *98*, 1358–1371. (d) Peterson, K. A.; Woon, D. E.; Dunning, T. H., Jr. *J. Chem. Phys.* **1994**, *100*, 7410–7415. (e) Wilson, A. K.; van Mourik, T.; Dunning, T. H., Jr. *J. Mol. Struct.: THEOCHEM* **1996**, *388*, 339–349.

(35) Descriptions of the Pople-type basis sets can be found in the following: Foresman, J. B.; Frisch, A. E. *Exploring Chemistry with Electronic Structure Methods*, 2nd ed.; Gaussian, Inc.: Pittsburgh, PA, 1996.

(36) Peterson, K. A.; Shepler, B. C.; Figgen, D.; Stoll, H. *J. Phys. Chem. A* **2006**, *110*, 13877–13883.

(37) McLean, A. D.; Chandler, G. S. *J. Chem. Phys.* **1980**, *72*, 5639–5648.

(38) Glukhovtsev, M. N.; Pross, A.; McGrath, M. P.; Radom, L. *J. Chem. Phys.* **1995**, *103*, 1878–1885.

(39) (a) Gonzalez, C.; Schlegel, H. B. *J. Chem. Phys.* **1989**, *90*, 2154–2161. (b) Gonzalez, C.; Schlegel, H. B. *J. Phys. Chem.* **1990**, *94*, 5523–5527.

(40) (a) Cizek, J. *Adv. Chem. Phys.* **1969**, *14*, 35–89. (b) Purvis, G. D., III; Bartlett, R. J. *J. Chem. Phys.* **1982**, *76*, 1910–1918. (c) Scuseria, G. E.; Janssen, C. L.; Schaefer, H. F., III. *J. Chem. Phys.* **1988**, *89*, 7382–7387. (d) Scuseria, G. E.; Schaefer, H. F., III. *J. Chem. Phys.* **1989**, *90*, 3700–3703. (e) Pople, J. A.; Head-Gordon, M.; Raghavachari, K. *J. Chem. Phys.* **1987**, *87*, 5968–5975.

(41) Lee, S.-H.; Liu, K. *J. Chem. Phys.* **1999**, *111*, 6253–6259.

(42) Jasper, A. W.; Klippenstein, S. J.; Harding, L. B. *J. Phys. Chem. A* **2010**, *114*, 5759–5768.

(43) Moore, C. E. *Atomic Energy Levels*; USGPO: Washington, DC, 1971; Vols. II and III, NSRDS-NBS 35.

(44) Feller, D.; Peterson, K. A.; de Jong, W. A.; Dixon, D. A. *J. Chem. Phys.* **2003**, *118*, 3510–3522.

(45) Shepler, B. C.; Balabanov, N. B.; Peterson, K. A. *J. Phys. Chem. A* **2005**, *109*, 10363–10372.

(46) *NIST Computational Chemistry Comparison and Benchmark Database*, NIST Standard Reference Database Number 101 Release February 15, 2010; Johnson, R. D., III, Ed.; 2010; http://cccbdb.nist.gov/.

(47) Stevens, J. E.; Cui, Q.; Morokuma, K. *J. Chem. Phys.* **1998**, *108*, 1544–1551.

(48) Singleton, D. L.; Cvetanovic, R. J. *J. Am. Chem. Soc.* **1976**, *98*, 6812–6819.

(49) (a) Eyring, H. *J. Chem. Phys.* **1935**, *3*, 107–115. (b) Johnston, H. S. *Gas Phase Reaction Rate Theory*; The Roland Press Co.: New York, 1966. (c) Laidler, K. J. *Theories of Chemical Reaction Rates*; McGraw-Hill: New

York, 1969. (d) Weston, R. E.; Schwartz, H. A. *Chemical Kinetics*; Prentice-Hall: New York, 1972. (e) Rapp, D. *Statistical Mechanics*; Holt, Reinhard, and Winston: New York, 1972. (f) Nikitin, E. E. *Theory of Elementary Atomic and Molecular Processes in Gases*; Claredon Press: Oxford, U.K., 1974. (g) Smith, I. W. M. *Kinetics and Dynamics of Elementary Gas Reactions*; Butterworths: London, 1980. (h) Steinfeld, J. I.; Francisco, J. S.; Hase, W. L. *Chemical Kinetics and Dynamics*; Prentice-Hall: Englewood Cliffs, NJ, 1989.

(50) Wigner, E. P. *Z. Phys. Chem.* **1932**, *B19*, 203–216.

(51) (a) Bell, R. P. *The Tunnel Effect in Chemistry*; Chapman and Hall: New York, 1980. (b) Louis, F.; Gonzalez, C.; Sawerysyn, J.-P. *J. Phys. Chem. A* **2004**, *108*, 10586–10593. (c) Zhu, L.; Bozzelli, J. W.; Kardos, L. M. *J. Phys. Chem. A* **2007**, *111*, 6361–6377. (d) Canneaux, S.; Louis, F.; Ribaucour, M.; Minetti, R.; El Bakali, A.; Pauwels, J.-F. *J. Phys. Chem. A* **2008**, *112*, 6045–6052.

(52) (a) Garrett, B. C.; Truhlar, D. G. *J. Phys. Chem.* **1979**, *83*, 2921–2926. (b) Garrett, B. C.; Truhlar, D. G. *J. Chem. Phys.* **1984**, *81*, 309–317. (c) Skodje, R. T.; Garrett, B. C.; Truhlar, D. G. *J. Phys. Chem.* **1981**, *85*, 3019–3023. (d) Skodje, R. T.; Garrett, B. C.; Truhlar, D. G. *J. Chem. Phys.* **1982**, *77*, 5955–5976. (e) Garrett, B. C.; Truhlar, D. G.; Grev, R. S.; Magnuson, A. W. *J. Phys. Chem.* **1980**, *84*, 1730–1748. (f) Garrett, B. C.; Truhlar, D. G.; Grev, R. S.; Magnuson, A. W. *J. Phys. Chem.* **1983**, *87*, 4554–4554.

(53) (a) Miller, W. H.; Shi, S.-H. *J. Chem. Phys.* **1981**, *75*, 2258–2264. (b) Miller, W. H.; Smith, F. T. *Phys. Rev.* **1978**, *A17*, 939–953.

(54) Henon, E.; Bohr, F.; Canneaux, S.; Postat, B.; Auge, F.; Bouillard, E.; Domureau, V. *KISTHEP 1.0*; University of Reims Champagne-Ardenne: France, 2003.

(55) Rayez, M. T.; Rayez, J. C.; Sawerysyn, J. P. *J. Phys. Chem.* **1994**, *98*, 11342–11352.

(56) Hammond, G. S. *J. Am. Chem. Soc.* **1955**, *77*, 334–338.

JP104163T